CROSS-SPECIES VS SPECIES-SPECIFIC MODELS FOR PROTEIN MELTING TEMPERATURE PREDICTION

A PREPRINT

Sebastián García López
Department of Computer Science - DIKU
University of Copenhagen
Sebastian.Garcia.Lopezs@di.ku.dk

Jesper Salomon
Novonesis
JRSX@novonesis.com

Wouter Boomsma
Department of Computer Science - DIKU
University of Copenhagen
wb@di.ku.dk

October 10, 2024

ABSTRACT

Protein melting temperatures are important proxies for stability, and frequently probed in protein engineering campaigns, including enzyme discovery, protein optimization, and de novo protein design. With the emergence of large datasets of melting temperatures for diverse natural proteins, it has become possible to train models to predict this quantity, and the literature has reported impressive performance values in terms of Spearman rho. The high correlation scores suggest that it should be possible to reliably predict melting temperature changes in engineered variants, to design de novo thermostable proteins, and identifying naturally thermostable proteins. However, in practice, results in this setting are often disappointing. In this paper, we explore the discrepancy between these two settings. We show that Spearman rho over cross-species data gives an overly optimistic impression of prediction performance, and that models trained on species-specific data often outperform larger cross-species models. Finally, we explore a number of strategies for improving performance, demonstrating a performance boost of 1.5 degree RMSE with fairly simple means.

Introduction

Reliable prediction of protein thermal stability is a long-standing challenge in protein engineering, particularly for enzyme optimization, where it is a strong indicator for functional integrity under thermal stress. Special focus has been on the prediction of the *changes* in stability induced by mutations, also referred to as $\Delta\Delta G$. Over the last decades, a long list of algorithms have been developed for this purpose, ranging from early models such as Delgado et al. [2019] and Rosetta Sora et al. [2023], to deep learning approaches based on convolutional and graph neural networks (Boomsma and Frellsen [2017], Li et al. [2020], Blaabjerg et al. [2023]), and most recently approaches building on large pre-trained models Dieckhaus et al. [2023].

Rather than considering *differences* in thermostability, other work has focused on predicting absolute stability Cagiada et al. [2024]. In this setting, the melting temperature, T_m of a protein is a useful proxy. It has the advantage that it can be measured reproducibly in high-throughput assays. Additionally, unlike other measures of protein stability or those that assess stability under specific conditions, the melting temperature is directly comparable across proteins, making it a valuable general optimization target, frequently correlating with stability to complex stress factors Sanchez-Ruiz [2010].

A recent large-scale dataset of melting temperature of 48,000 proteins across 13 species Jarzab et al. [2020], combined with standardized splits Dallago et al. [2021], has made the T_m prediction problem accessible to the machine learning community. Several recent studies have reported impressive prediction performance, with Spearman correlation coefficients above 0.7 Dallago et al. [2021], Su et al. [2023], Sułek et al. [2024], Rodella et al. [2024], Pudžiuvelytė et al. [2024], Li et al. [2023], Yang et al. [2022].

Although progress in this area are highly welcome, the high performance values reported in the literature are somewhat at odds with our expectation about the difficulty of this prediction task. Generally, absolute stability prediction has been

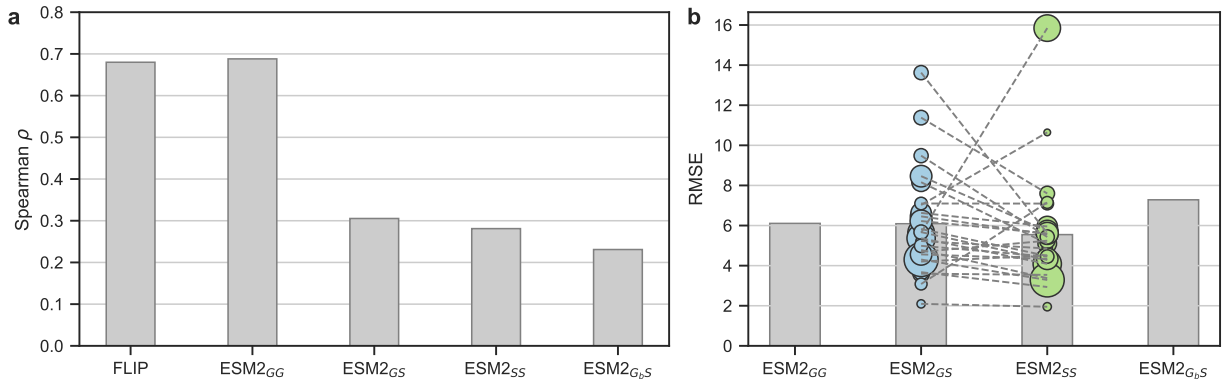

Figure 1: Performance of sequence based embeddings to predict melting temperature across species. a) Performance measured in terms of Spearman rank correlation, b) Performance measured in terms of RMSE, showing the individual performances per species as circles, scaled by the size of the dataset. The G and S subscripts denote *global*, and *specifies-specific*, respectively, with the first denoting the training scenario and the second denoting the testing scenario. For instance *GS* denotes a model trained on all data, while being evaluated on each species. G_B denotes a model that where the dataset was balanced by species during training (see Method). Note how much of the correlation arises simply from the fact that the correlation is measured across all species.

considered to be more challenging that relative stability prediction. In addition, it conflicts with our own prior experience with melting temperature prediction in the protein engineering setting, where we have typically seen substantially lower performances than those reported Notin et al. [2023]. In this paper, we investigate the origin of this apparent discrepancy as a stepping stone towards a better understanding of the status of prediction performance in this domain. We start by identifying the basis for the performance discrepancy – and show that much of the reported Spearman correlation arises as the consequence of the difference in melting temperature between species, rather than an ability to predict melting temperatures for individual variants. We thus confirm that species-specific melting temperature remains a challenging problem, with current methods displaying RMS errors of about 6 degrees, which are substantial, given the inner-species variance. Next, we ask the question whether greater performance can be obtained by training species-specific models, rather than a single large cross-species model. We then pursue three potential strategies for increasing performance further, using 1) a richer input embedding, 2) a representation obtained from a constrastive training objective, and 3) a loss that explicitly anchors the results to the optimal growth temperature of the species. Ultimately, our results show that the species-specific models maintain their edge over the cross-species models in these different settings, and that prediction errors can be reduced by about 1.5 degree RMSE with fairly simple means.

Results

We start by establishing a simple model architecture as a baseline for our subsequent analyses. The model takes ESM-2 embeddings Lin et al. [2022] as input, and produces melting temperature values as output. For simplicity, we use a classic transfer-learning setup with frozen embeddings (no fine-tuning). To aggregate the per-position embeddings into a single output we use a light attention layer, as this is known to outperform simple averaging over the length of the protein Stärk et al. [2021], Detlefsen et al. [2022]. Running on the standard splits of the Meltome dataset, our baseline method marginally outperform the results reported in the original FLIP paper (Figure 1a, two left-most bars), demonstrating that our baseline implementation serves as a reasonable representative of the current state of the art. See *Methods* for details.

Discrepancy explained: correlation is a poor metric

The third bar in Figure 1a (ESM2$_{GS}$) is equivalent to the second, but evaluates the Spearman correlation for each specifies individually and reports the average. The dramatic difference of this result compared to the two first bars explains the discrepancy discussed above. Clearly, much of the observed correlation found in the first two bars is due simply to global melting temperature differences between species, rather than the ability to determine melting temperature differences for different proteins within a species. This suggests that basing conclusions solely on the correlation of predictions with the ground truth may lead to misleading conclusions, and highlights the need to include

additional metrics in the assessment of model performance. To illustrate, if we instead measure our performance in terms of root mean square error (RMSE), we find no notable discrepancy between the cross-species and per-species assessment of our model (1b). In the remainder of this paper, we will therefore rely on RMSE for our conclusions.

Species-specific models potentially outperform cross-species models

We have established that evaluating performance per-species aligns more closely with the objective of interest, namely assessing the impact of variation within species. A natural question is whether *training* separate models on each species is also beneficial. Although cross-species models are convenient, there are situations where species-specific models would be equally useful. One important use-case is for the surrogate function in a Bayesian optimization framework. In this setting, we typically have observed data for the specific system, and wish to generalize to unseen variants, potentially updating the model when new experimental data is observed. The training of cross-species vs species-specific models represents a trade-off. On one hand, one might expect that cross-species models could benefit from larger datasets and could provide greater generalization capabilities; on the other hand, a specialized species-specific model might obtain a better fit with fewer parameters.

Assessing this question empirically on the FLIP dataset, we see that training separate models on each species (ESM2$_{SS}$, 1a, fourth column) provides comparable performance to the global model, suggesting that training larger cross-species models is not beneficial in this setting, perhaps even showing slight detrimental effects in terms of RMSE. We note that the lack of performance of the global model is not related to the imbalance of data set sizes between species. In fact, rebalancing the databaset during training leads to worse results (ESM2$_{G_bS}$). Instead, the problem is likely related to the same behavior that led to the exaggerated performance when measured with Spearman correlation: a Simpson-paradox like issue, where the model focuses on the global trends and disregard the local intra-species effects.

When tracking the performance differences on the individual data sets (Figure 1b, middle two columns), we see that there is actually a general trend towards better performance when training species-specific models, but that these models show greater variance across species (see also Appendix A, C, D). Interestingly, while the outliers for the global model are typically the smaller datasets as one would expect, the species-specific models sometimes fail even on species with abundant data. This suggests that there is potential for performance improvement in the species-specific models if we can find ways to mitigate the variance issues. In the following, we will pursue three different strategies towards this goal.

Strategy 1: Richer featurizations

We hypothesize that one way to reduce variance and improve the reliability of predictions is to enrich the input featurization by incorporating information derived from protein structures. For this reason, in addition to using sequence-based embeddings (ESM2), we included embeddings generated by the PiFold inverse folding model (Figure 2C and *Methods*). The idea is that concatenation of sequence and protein structure embeddings provides a more expressive representation, potentially allowing for improved prediction.

Figure 4a demonstrates the performance for global and species-specific models using the two input embeddings, for clarity allocating the y-axis for the individual species. The combined ESM2+Pifold embedding is indeed observed to reduce the variance of the species specific models, avoiding the critical outliers observed for the ESM2 embedding and generally displaying improved performance across species. Interestingly, the global model produces *more* outliers with the combined embedding, although this effect seems to be limited to the species for which we have very little training data.

Strategy 2: Contrastive learning

The results above suggest that the global model focuses on the differences in optimal growth temperature (OGT) between species, rather than the effect of individual variants. We therefore considered whether we could choose alternative training objectives that better reflected our desired outcomes.

One intuitively appealing approach is *contrastive* learning, where a model is trained to enforce pairwise relationships between samples, for instance ensuring that proximal neighbors belong to the same class. Often, such methods will use data augmentation strategies to produce local variations that are considered proximal, and can then be contrasted with all other points in terms of the predicted output values. In the field of image processing, data augmentation often consists of various transformation techniques, such as cropping, resizing, Gaussian noise addition and rotations Chen et al. [2020]. The effectiveness of this approach depends on the expressiveness of such transformations. Overly conservative, trivial augmentation might result in lack of generalization, while overly broad augmentation produces false negative samples Chuang et al. [2020],Khosla et al. [2020].

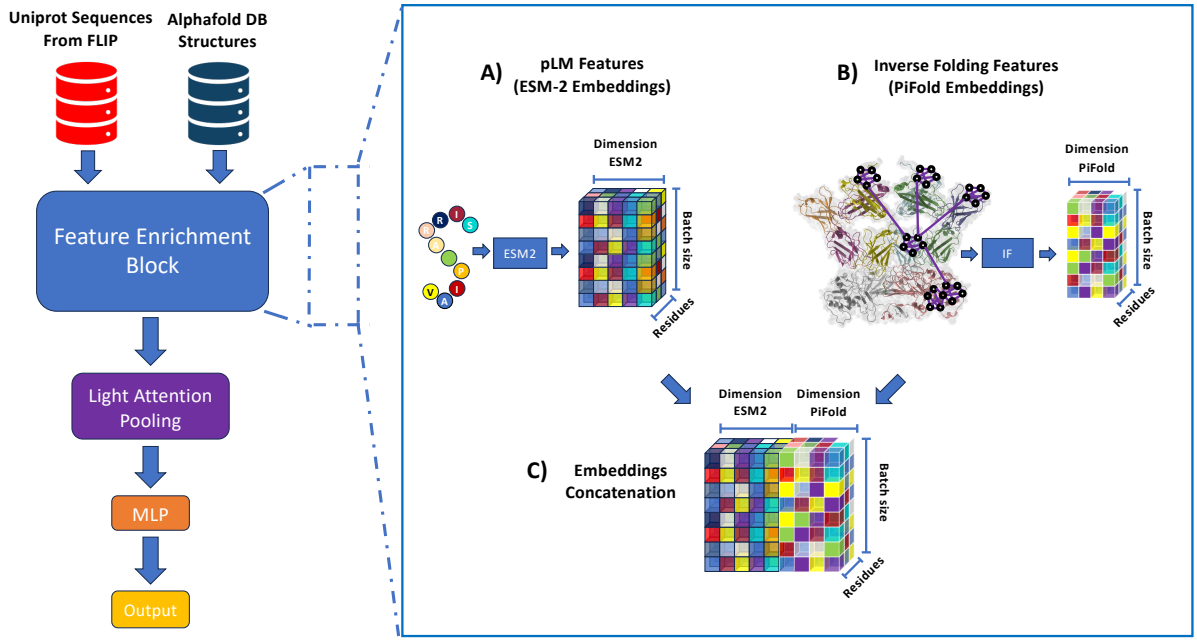

Figure 2: The methodological approach in this study utilizes embeddings derived from protein language models, specifically ESM2 and PiFold, or a combination thereof (see Figure 2). Subsequently, a Light Attention (LA) block is implemented to perform appropriate pooling of these embeddings. Given the variability in sequence length among proteins in the dataset across organisms, the LA block is particularly suitable. Unlike conventional pooling methods, the LA block processes embeddings by channel using convolutional neural networks (CNNs), rather than based on embedding length. This block performs learned pooling, capturing features extracted by the embedding and generating a condensed representation of the initial set of embeddings for each protein. This condensed representation then serves as input features for a multilayer perceptron (MLP) regressor to predict melting temperatures (t_m).

For the purpose of T_m prediction, there are two challenges in applying contrastive learning: 1) there is no trivial data augmentation procedure available, 2) we are in a regression-setting rather than a classification setting. A recent approach, rank-N-contrast Zha et al. [2024], presents a solution to both problems, by using a contrastive learning objective to learn a representation of the inputs, which can subsequently be used as input for a downstream regression task. This method was shown to be insensitive to the choice of data augmentation (it can be applied even without it), and the two-step procedure makes is amenable for regression. To learn the representation, the rank-N-contrast method contrasts samples based on their ranking within the target space of continuous labels. For example, if two samples in a batch during training have the highest similarity in terms of melting temperature, they will be enforced to have the shortest distance in representation space. Given the beneficial role of data augmentation in the original paper, we add a simple data augmentation step in the form of a small Gaussian perturbation of the embedding input vector. Once the representations are learned, they are used directly as input to the multilayer perceptron regressor (MLP), replacing the feature enrichment and light attention blocks in Figure 2. See *Method* for details.

The results for the contrastive learing experiments are report in Figure 4b. While the contrastive method produces reasonable results, they are clearly inferior to our initial MSE strategy.

Strategy 3: Anchoring to optimal growth temperature

A simpler strategy towards an improved focus on in-species differences is to use centroids to condition learning over each species or mode in the distributions. Each centroid represents the average melting temperature (μ_{t_m}) of the proteins belonging to a particular species. The purpose of these centroids is to prevent the represented proteins from deviating from their corresponding distributions. In practical terms, the average t_m of each species would serve as the Optimal Growth Temperature (OGT) for the proteins of that species. In the context of thermostability, optimal growth temperature (OGT) is an indirect measure of the ability of proteins and biomolecules to maintain their essential functions and structural integrity (i.e. remain stable) in high temperature environments. This measure is reflected in the behaviour of organisms (micro-organisms) when exposed to elevated temperatures just prior to denaturation.

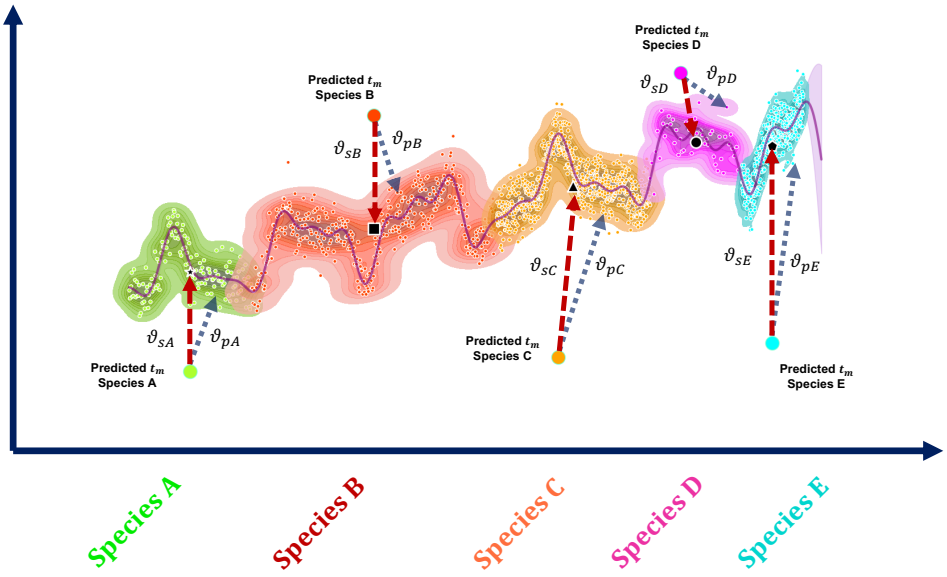

Figure 3: Mechanism of action of the dual loss function. In the graph, the densities represent the space of continuous labels corresponding to the t_m of each protein within the training set. Each density is indicated by a specific colour, which indicates the species to which the points within that density belong. The purple line through all densities depicts the trend of t_m over the continuous label space. Points outside the densities are the t_m predicted by the model and are indicated by colours indicating their membership of a particular species, where the predicted t_m is a linear combination of the predicted OGT and its bias (see equation 1). The dashed blue arrows represent the MSE between the predicted sample and its ground truth t_m, while the red arrows correspond to the MSE between the predicted OGT and the centroid in the respective density, which acts as the estimated OGT or true value for practical purposes. In addition, it is important to consider practical issues, e.g. that μ_{t_m} is only needed during the training stage, so that this information is not needed during inference. Furthermore, the calculation of μ_{t_m} is done beforehand by averaging the t_m per species in the training and validation sets, and is then used during the training process. Therefore, during the induction process, it is necessary to have information about the species to which the protein belongs and its associated t_m.

Figure 3 illustrates the operation of the loss function. This mechanism is based on conditioning the t_m predictions of each protein to values within the ranges determined by the Optimal Growth Temperature (OGT) of each species. This is achieved by contrasting the predictions with the centroids calculated previously by averaging the t_m per species used as estimated OGTs. This procedure can be considered as a regularisation mechanism during optimisation, as it attempts to avoid predictions that deviate significantly from the expected values according to the OGTs. The loss function is defined as:

$$\mathcal{L}_{\text{dual}} = \vartheta_p(\varphi_{t_m}, y_{t_m}) + \vartheta_s(\tilde{y}_{OGT}, \mu_{t_m}) \quad \text{where} \quad \varphi_{t_m} = \tilde{y}_{OGT} + \tilde{y}_{bias} \tag{1}$$

Here, φ_{t_m} the predicted t_m output from the model (see Figure 2), y_{t_m} denotes the ground truth melting temperature, $\tilde{y}_{OGT}$ is the predicted OGT for each sample, μ_{t_m} is the average t_m per species, ϑ_p is the mean square error (MSE) between the predicted φ_{t_m} and the ground truth t_m, and ϑ_s is the MSE between the predicted OGT and the average t_m per species. A visual illustration of the procedure is presented in figure 3. During training, values for the average and the deviation are specified separately, but this training scheme maintains the advantage that no information about OGT (or average melting temperature) is necessary at test time.

Our experiments on the FLIP dataset are reported in Figure 4c. The dual-loss approach provides some improvement for the global model for the structurally enriched ESM+PiFold input representation, but it does not fully close the gap between the global and species-specific models, with the latter still displaying a slight edge. Perhaps surprisingly at first sight, we note that the species-specific model also benefits from the dual-loss strategy, although in this case, the average loss is simply a constant value for all data points in the training set. The explanation for this phenomenon is found in the fact that the dual loss implicitly standardizes the output values (from global melting temperatures to deviations from an average). The dual loss strategy can thus be viewed as a meaningful standardization technique that can be applied in the global setting, where standard standardization techniques would fail (since a global mean is not a meaningful anchor), while corresponding to a standard substraction of the mean in the single-species case.

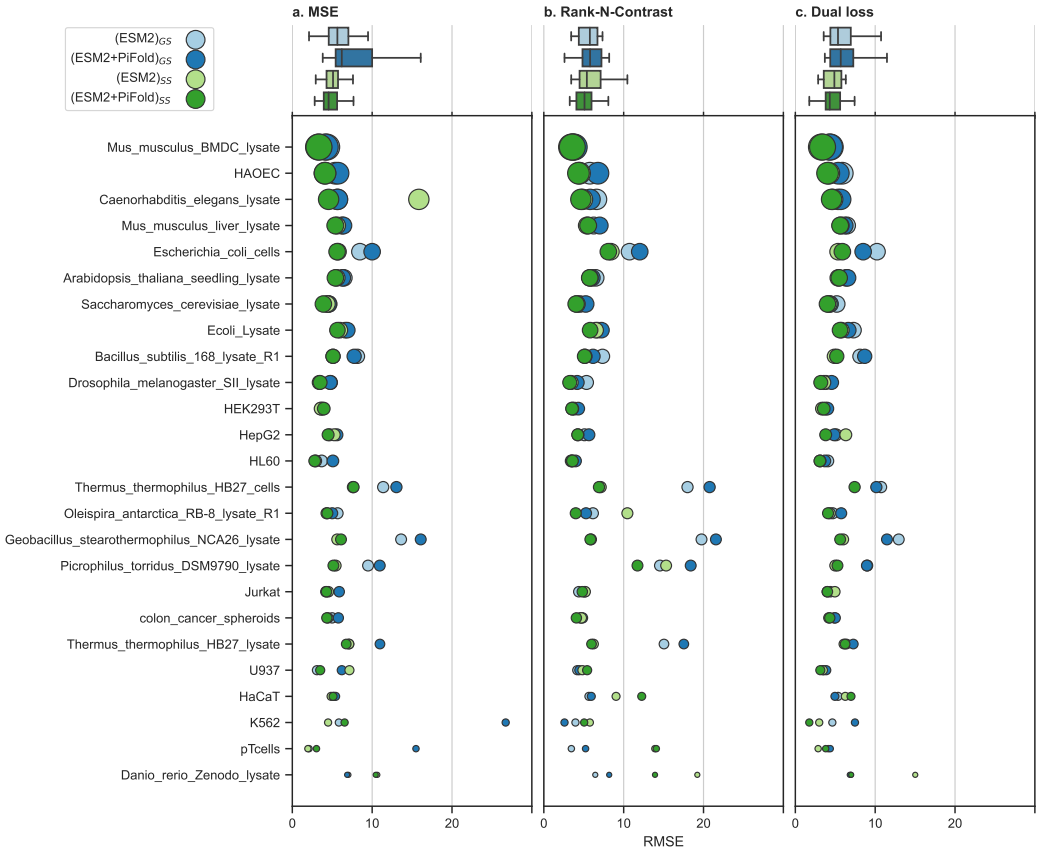

Figure 4: Results on the FLIP Meltome dataset for the three strategies discussed in the main text. For each strategy, the figure contrasts the performance of sequence-based embeddings (light colors) vs. the combination of sequence-based embeddings and protein structurederived embeddings (full colors) in terms of RMSE.

	Global		**Species-specific**	
	ESM_{gs}	**$(ESM + PiFold)_{gs}$**	**ESM_{ss}**	**$(ESM + PiFold)_{ss}$**
MSE	5.90	6.34	5.99	4.59
Rank-N-contrast	6.78	7.21	5.63	5.08
Dual loss	5.95	5.86	7.21	**4.53**

Table 1: Overview of results in terms of an average over RMSE for the individual datasets, weighted by test-set size. **ss** denotes individual models per species, while **gs** represents global models applied to each species. The methods compared include traditional approaches based on loss functions such as Mean Squared Error (MSE) or sample balancing per batch using the same loss function, as compared to contrastive methods such as Rank N Contrast Loss (Rank N) and the dual loss (biasg) proposed in this study.

Discussion

A summary of the results can be found in Table 1. In short, we find that species-specific models generally outperform globally trained models. Species-specific models suffer from larger variance on small datasets, but it appears that this effect can be mitigated by expanding the input embedding to include structural information, presumably serving as a regularizer to guard against overfitting. Somewhat unexpectedly, the inclusion of structural information was not beneficial in the global training scheme.

The Rank-N-contrast and Dual loss approaches can both be viewed as examples of contrastive learning methods. The former learns a representation by contrasting inputs within a small perturbation region with the rest, while the latter is a simple strategy where predictions are anchored to the species mean. In our hands, the rank-N-contrast method did not provide any useful performance gains, but this could be due to the choice of perturbation mechanism used. When combined with the enriched featurization, the dual loss ultimately produces the best results, but they differ only marginally from the results obtained with MSE on the (ESM + PiFold) input embedding. As discussed earlier, we stress that when employed in the species-specific setting, the dual loss merely corresponds to a mean standardization.

The overall conclusion is that the performance of thermal stability prediction can be improved by almost 1.5 degrees RMSE using fairly simple techniques. In particular, the choice of training species-specific models rather than global models had an important effect, but only when also combined with a enriched input featurization that incorporates structural information.

Methods

Embedding types Our model employs two different embedding types: a sequence-based embedding from the ESM2 (Evolutionary Scale Modeling) model Lin et al. [2022] and an embedding obtained from the inverse folding model PiFold Hsu et al. [2022]. The former is an unsupervised language model based on the transformer architecture, trained on 250 million sequences from the UniRef dataset, which has been shown to capture and learn relevant information such as biochemical properties of amino acids, residue contact mapping, and homology detection, making it well-suited for various downstream tasks Rives et al. [2021], Lin et al. [2022], Michael et al. [2024]. As an inverse folding method, PiFold aims to predict protein sequences based on the atomic coordinates of protein backbone structures, and thus more directly captures the structural environment in its embeddings.

Model design The fundamental structure of the model is illustrated in Figure 2. The sequence and structural embeddings produce per-residue vector representations of 1280 and 128 dimensions respectively. These were either used independently or concatenated per residue, and passed through a light attention block (see Figure 2). As the name suggests, light attention is a light-weight mechanism to approximate a traditional attention mechanism, and is commonly used as an alternative to simpler aggregation options such as calculating a mean over the sequence length Stärk et al. [2021]. This approach allows a unified and efficient representation of protein features, regardless of sequence length. While the Feature Enrichment Block performs the embeddings pre-processing during the induction/inference phase of the model, the Light Attention Block acts as an encoder, learning a compact representation of the features in the embedding space. This condensed representation is then fed into a single dense neural network which performs regression to predict melting temperature values.

The light attention block was implemented using the default parameters as described in Stärk et al. [2021], although dimensionality of the input embeddings was adjusted based on the type of embedding used. For prediction, a multilayer perceptron (MLP) was designed, comprising three hidden layers with an architecture of (128, 64, n), where n represents the number of output components, which varies depending on the specific experiment. This configuration allows for model adaptability to different predictive tasks while maintaining a consistent base structure.

Rank-N-Contrast The Rank-N-Contrast Zha et al. [2024] procedure consists of 3 components:

Data augmentation: A batch of input-label pairs undergoes data augmentation in the original embedding space using a Gaussian perturbation. While the original description of the method proposed constructing a two-view batch consisting of two types of augmentations, we deviate slightly from this by creating a two-view batch which comprises the original input and a transformed version of the same input. In our case, the transformation was implemented as a Gaussian perturbation in the embedding space.

Rank-N-Contrast Loss: A regression-aware loss function is constructed to learn a representation of the input data such that relative distances reflect differences in their continuous target values (i.e. melting temperatures). Following the original publication, the $\mathrm{R}_N\mathrm{C}$ loss per sample is defined as:

$$l_{\text{RNC}}^{(i)} = \frac{1}{2N-1} \sum_{j=1, j\neq i}^{2N} -\log \mathbb{P}(v_j|v_i, \mathcal{S}_{i,j}) \qquad \text{where} \qquad \mathbb{P}(v_j|v_i, \mathcal{S}_{i,j}) = \frac{\exp(\text{sim}(v_i, v_j)/\tau)}{\sum_{v_k \in \mathcal{S}_{i,j}} \exp(\text{sim}(v_i, v_k)/\tau)}$$

Here, $\text{sim}(\cdot,\cdot)$ is a similarity in representation-space between samples v_i and v_j, and τ is a temperature parameter. $\mathbb{P}(v_j|v_i, \mathcal{S}_{i,j})$ represents the likelihood of a sample v_j in the context of anchor v_i, and the set of samples $\mathcal{S}_{i,j})$ that relative to v_i have a worse rank than v_j in terms of the *output* values.

$$\mathcal{S}_{i,j} := \{v_k \mid k \neq i, d(\tilde{y}_i, \tilde{y}_k) \geq d(\tilde{y}_i, \tilde{y}_j)\}$$

As an example, if v_j is the sample that is closest to v_i in terms of melting temperature, the likelihood would be optimized when v_j had the highest similarity to v_i in representation space. The full likelihood is simply an average over all samples in the batch.

$$\mathcal{L}_{\text{RNC}} = \frac{1}{2N} \sum_{i=1}^{2N} l_{\text{RNC}}^{(i)}$$

Representation Learning: The model learns an encoder by optimizing $\mathcal{L}_{\text{RNC}}$. Once the representation is learned, the encoder is frozen, and a separate predictor is trained using a standard loss. In our case, the learned Rank-N-Contrast representations are used as direct input to the light attention block in figure 2.

Data All analyses were done on the Meltome partition of the FLIP dataset Dallago et al. [2021]. The dataset comprises 15 partitions designed to address various tasks in the field of protein design. For this study, we specifically focused on the partition related to thermostability, based on proteins with their corresponding melting temperatures (t_m) derived from the Meltome Atlas database. The 'Mix' partition was selected, characterized by a high diversity of proteins originating from multiple species. Proteins less than 50 residues in length were discarded for this work. The amount of proteins corresponding to each species in the splits of the FLIP dataset is presented in the Table 2

	Sample Size		
Species	**Train**	**Val**	**Test**
Mus musculus BMDC lysate	3108	369	227
HAOEC	2157	242	488
Caenorhabditis elegans lysate	1900	195	350
Mus musculus liver lysate	1308	139	71
Escherichia coli cells	1254	133	49
Arabidopsis thaliana seedling lysate	1252	139	203
Saccharomyces cerevisiae lysate	1245	123	226
Ecoli Lysate	1108	137	212
Bacillus subtilis 168 lysate R1	931	91	158
Drosophila melanogaster SII lysate	895	103	152
HEK293T	735	76	123
HepG2	647	71	85
HL60	628	79	82
Thermus thermophilus HB27 cells	573	59	58
Oleispira antarctica RB 8 lysate R1	555	77	125
Geobacillus stearothermophilus NCA26 lysate	541	68	36
Picrophilus torridus DSM9790 lysate	539	53	138
Jurkat	499	53	49
colon cancer spheroids	486	50	74
Thermus thermophilus HB27 lysate	426	47	105
U937	380	29	16
HaCaT	293	42	33
K562	237	28	2
pTcells	185	24	3
Danio rerio Zenodo lysate	119	11	11

Table 2: Sample distribution table by species. This table was constructed based on the distribution provided by the flip partition in relation to the Meltome Atlas, using the crossspecies partition or "mix".

Protein sequences from FLIP split were used to compute embeddings using ESM2, which were then stored in files for efficient loading during model induction/inference. To map structural features, the UniProtIDs of each protein were used as a query in AlphaFoldDB Varadi et al. [2022] to obtain predicted structures. This approach was adopted to ensure the use of the closest predicted protein structure for each sequence, while avoiding the complexity associated with multi-chain protein structures. Once the protein structures were obtained, PiFold was used to generate graph embeddings, which were then stored in files. Notably, only the encoder component of the algorithm was used, with the decoder omitted for practical reasons.

Training The training approach follows the principle of classic transfer learning, where the embeddings were pre-generated and not fine-tuned on the thermostability task. This strategy was chosen for its versatility and scalability to larger datasets, in addition to the fact that fine-tuning does not always improve performance and can be counterproductive Dieckhaus et al. [2023].

AdamW was used as the main optimiser. The learning rate (lr) was adjusted according to the type of experiment: for the calibration of models using the full FLIP training partition in the global model (all species in the dataset), $\text{lr} = 1 \times 10^{-4}$ was set, while for the training of species-specific models (individual models trained with proteins belonging to the same species), $\text{lr} = 1 \times 10^{-3}$ was used.

Due to its particular architecture, the Rank N Contrast model followed a different procedure.. This method requires a previously trained encoder to generate the representation (in this case, the light attention module) and a predictor (the multilayer dense neural network). The two components were optimised with different learning rates, denoted as lr_e (encoder) and lr_p (decoder). For global model calibration, $\text{lr}_e = 1 \times 10^{-5}$ and $\text{lr}_p = 1 \times 10^{-4}$, while for species-specific models, $\text{lr}_e = 1 \times 10^{-5}$ and $\text{lr}_p = 1 \times 10^{-3}$.

Acknowledgement

This project has received funding from the European Union's Horizon 2020 research and innovation programme under the Marie Sklodowska-Curie grant agreement No 801199, the Novo Nordisk Foundation through the MLSS Center (Basic Machine Learning Research in Life Science, NNF20OC0062606), and the Pioneer Centre for AI (DNRF grant number P1). The project was carried out in collaboration with the Enzyme Research Division of Novonesis A/S, located in Kongens Lyngby, Denmark.

References

Javier Delgado, Leandro G Radusky, Damiano Cianferoni, and Luis Serrano. FoldX 5.0: working with RNA, small molecules and a new graphical interface. *Bioinformatics*, 35(20):4168–4169, 03 2019. ISSN 1367-4803. doi:10.1093/bioinformatics/btz184. URL `https://doi.org/10.1093/bioinformatics/btz184`.

Valentina Sora, Adrian Otamendi Laspiur, Kristine Degn, Matteo Arnaudi, Mattia Utichi, Ludovica Beltrame, Dayana De Menezes, Matteo Orlandi, Ulrik Kristoffer Stoltze, Olga Rigina, Peter Wad Sackett, Karin Wadt, Kjeld Schmiegelow, Matteo Tiberti, and Elena Papaleo. Rosettaddgprediction for high-throughput mutational scans: From stability to binding. *Protein Science*, 32(1):e4527, 2023. doi:https://doi.org/10.1002/pro.4527. URL `https://onlinelibrary.wiley.com/doi/abs/10.1002/pro.4527`.

Wouter Boomsma and Jes Frellsen. Spherical convolutions and their application in molecular modelling. *Advances in neural information processing systems*, 30, 2017.

Bian Li, Yucheng T Yang, John A Capra, and Mark B Gerstein. Predicting changes in protein thermostability upon point mutation with deep 3d convolutional neural networks. *bioRxiv*, 2020.

Lasse M Blaabjerg, Maher M Kassem, Lydia L Good, Nicolas Jonsson, Matteo Cagiada, Kristoffer E Johansson, Wouter Boomsma, Amelie Stein, and Kresten Lindorff-Larsen. Rapid protein stability prediction using deep learning representations. *Elife*, 12:e82593, 2023.

Henry Dieckhaus, Michael Brocidiacono, Nicholas Randolph, and Brian Kuhlman. Transfer learning to leverage larger datasets for improved prediction of protein stability changes. *bioRxiv*, 2023.

Matteo Cagiada, Sergey Ovchinnikov, and Kresten Lindorff-Larsen. Predicting absolute protein folding stability using generative models. *bioRxiv*, pages 2024–03, 2024.

Jose M Sanchez-Ruiz. Protein kinetic stability. *Biophysical chemistry*, 148(1-3):1–15, 2010.

Anna Jarzab, Nils Kurzawa, Thomas Hopf, Matthias Moerch, Jana Zecha, Niels Leijten, Yangyang Bian, Eva Musiol, Melanie Maschberger, Gabriele Stoehr, et al. Meltome atlas—thermal proteome stability across the tree of life. *Nature methods*, 17(5):495–503, 2020.

Christian Dallago, Jody Mou, Kadina E Johnston, Bruce J Wittmann, Nicholas Bhattacharya, Samuel Goldman, Ali Madani, and Kevin K Yang. Flip: Benchmark tasks in fitness landscape inference for proteins. *bioRxiv*, pages 2021–11, 2021.

Jin Su, Chenchen Han, Yuyang Zhou, Junjie Shan, Xibin Zhou, and Fajie Yuan. Saprot: Protein language modeling with structure-aware vocabulary. *bioRxiv*, pages 2023–10, 2023.

Adam Sułek, Jakub Jończyk, Patryk Orzechowski, Ahmed Abdeen Hamed, and Marek Wodziński. Esmtemp - transfer learning approach for predicting protein thermostability. In *Computational Science – ICCS 2024: 24th International Conference, Malaga, Spain, July 2–4, 2024, Proceedings, Part III*, page 187–194, Berlin, Heidelberg, 2024. Springer-Verlag. ISBN 978-3-031-63758-2. doi:10.1007/978-3-031-63759-9_23. URL `https://doi.org/10.1007/978-3-031-63759-9_23`.

Chiara Rodella, Symela Lazaridi, and Thomas Lemmin. TemBERTure: advancing protein thermostability prediction with deep learning and attention mechanisms. *Bioinformatics Advances*, 4(1):vbae103, 07 2024. ISSN 2635-0041. doi:10.1093/bioadv/vbae103. URL `https://doi.org/10.1093/bioadv/vbae103`.

Ieva Pudžiuvelytė, Kliment Olechnovič, Egle Godliauskaite, Kristupas Sermokas, Tomas Urbaitis, Giedrius Gasiunas, and Darius Kazlauskas. TemStaPro: protein thermostability prediction using sequence representations from protein language models. *Bioinformatics*, 40(4):btae157, April 2024. ISSN 1367-4811. doi:10.1093/bioinformatics/btae157. URL `https://doi.org/10.1093/bioinformatics/btae157`.

Mengyu Li, Hongzhao Wang, Zhenwu Yang, Longgui Zhang, and Yushan Zhu. Deeptm: A deep learning algorithm for prediction of melting temperature of thermophilic proteins directly from sequences. *Computational and Structural Biotechnology Journal*, 21:5544–5560, 2023. ISSN 2001-0370. doi:https://doi.org/10.1016/j.csbj.2023.11.006. URL `https://www.sciencedirect.com/science/article/pii/S2001037023004221`.

Yang Yang, Jianjun Zhao, Lianjie Zeng, and Mauno Vihinen. Protstab2 for prediction of protein thermal stabilities. *International Journal of Molecular Sciences*, 23(18), September 2022. ISSN 1661-6596. doi:10.3390/ijms231810798.

Pascal Notin, Aaron Kollasch, Daniel Ritter, Lood van Niekerk, Steffanie Paul, Han Spinner, Nathan Rollins, Ada Shaw, Rose Orenbuch, Ruben Weitzman, Jonathan Frazer, Mafalda Dias, Dinko Franceschi, Yarin Gal, and Debora Marks. Proteingym: Large-scale benchmarks for protein fitness prediction and design. In A. Oh, T. Neumann, A. Globerson, K. Saenko, M. Hardt, and S. Levine, editors, *Advances in Neural Information Processing Systems*, volume 36, pages 64331–64379. Curran Associates, Inc., 2023. URL `https://proceedings.neurips.cc/paper_files/paper/2023/file/cac723e5ff29f65e3fcbb0739ae91bee-Paper-Datasets_and_Benchmarks.pdf`.

Zeming Lin, Halil Akin, Roshan Rao, Brian Hie, Zhongkai Zhu, Wenting Lu, Allan dos Santos Costa, Maryam Fazel-Zarandi, Tom Sercu, Sal Candido, et al. Language models of protein sequences at the scale of evolution enable accurate structure prediction. *BioRxiv*, 2022:500902, 2022.

Hannes Stärk, Christian Dallago, Michael Heinzinger, and Burkhard Rost. Light attention predicts protein location from the language of life. *Bioinformatics Advances*, 1(1):vbab035, 2021.

Nicki Skafte Detlefsen, Søren Hauberg, and Wouter Boomsma. Learning meaningful representations of protein sequences. *Nature communications*, 13(1):1914, 2022.

Ting Chen, Simon Kornblith, Mohammad Norouzi, and Geoffrey Hinton. A simple framework for contrastive learning of visual representations. In *International conference on machine learning*, pages 1597–1607. PMLR, 2020.

Ching-Yao Chuang, Joshua Robinson, Yen-Chen Lin, Antonio Torralba, and Stefanie Jegelka. Debiased contrastive learning. *Advances in neural information processing systems*, 33:8765–8775, 2020.

Prannay Khosla, Piotr Teterwak, Chen Wang, Aaron Sarna, Yonglong Tian, Phillip Isola, Aaron Maschinot, Ce Liu, and Dilip Krishnan. Supervised contrastive learning. *Advances in neural information processing systems*, 33: 18661–18673, 2020.

Kaiwen Zha, Peng Cao, Jeany Son, Yuzhe Yang, and Dina Katabi. Rank-n-contrast: learning continuous representations for regression. *Advances in Neural Information Processing Systems*, 36, 2024.

Chloe Hsu, Robert Verkuil, Jason Liu, Zeming Lin, Brian Hie, Tom Sercu, Adam Lerer, and Alexander Rives. Learning inverse folding from millions of predicted structures. In *International Conference on Machine Learning*, pages 8946–8970. PMLR, 2022.

Alexander Rives, Joshua Meier, Tom Sercu, Siddharth Goyal, Zeming Lin, Jason Liu, Demi Guo, Myle Ott, C Lawrence Zitnick, Jerry Ma, et al. Biological structure and function emerge from scaling unsupervised learning to 250 million protein sequences. *Proceedings of the National Academy of Sciences*, 118(15):e2016239118, 2021.

Richard Michael, Jacob Kæstel-Hansen, Peter Mørch Groth, Simon Bartels, Jesper Salomon, Pengfei Tian, Nikos S Hatzakis, and Wouter Boomsma. A systematic analysis of regression models for protein engineering. *PLOS Computational Biology*, 20(5):e1012061, 2024.

Mihaly Varadi, Stephen Anyango, Mandar Deshpande, Sreenath Nair, Cindy Natassia, Galabina Yordanova, David Yuan, Oana Stroe, Gemma Wood, Agata Laydon, et al. Alphafold protein structure database: massively expanding the structural coverage of protein-sequence space with high-accuracy models. *Nucleic acids research*, 50(D1): D439–D444, 2022.

Suplementary Material

The supplementary material presented below includes supporting results for all experiments conducted in this study. This material includes violin plots and box plots for all methods and performance measures analysed in the paper, as well as tables with the corresponding results from the cross-species analysis.

A Violin and Box Plots of Predictions Across Species

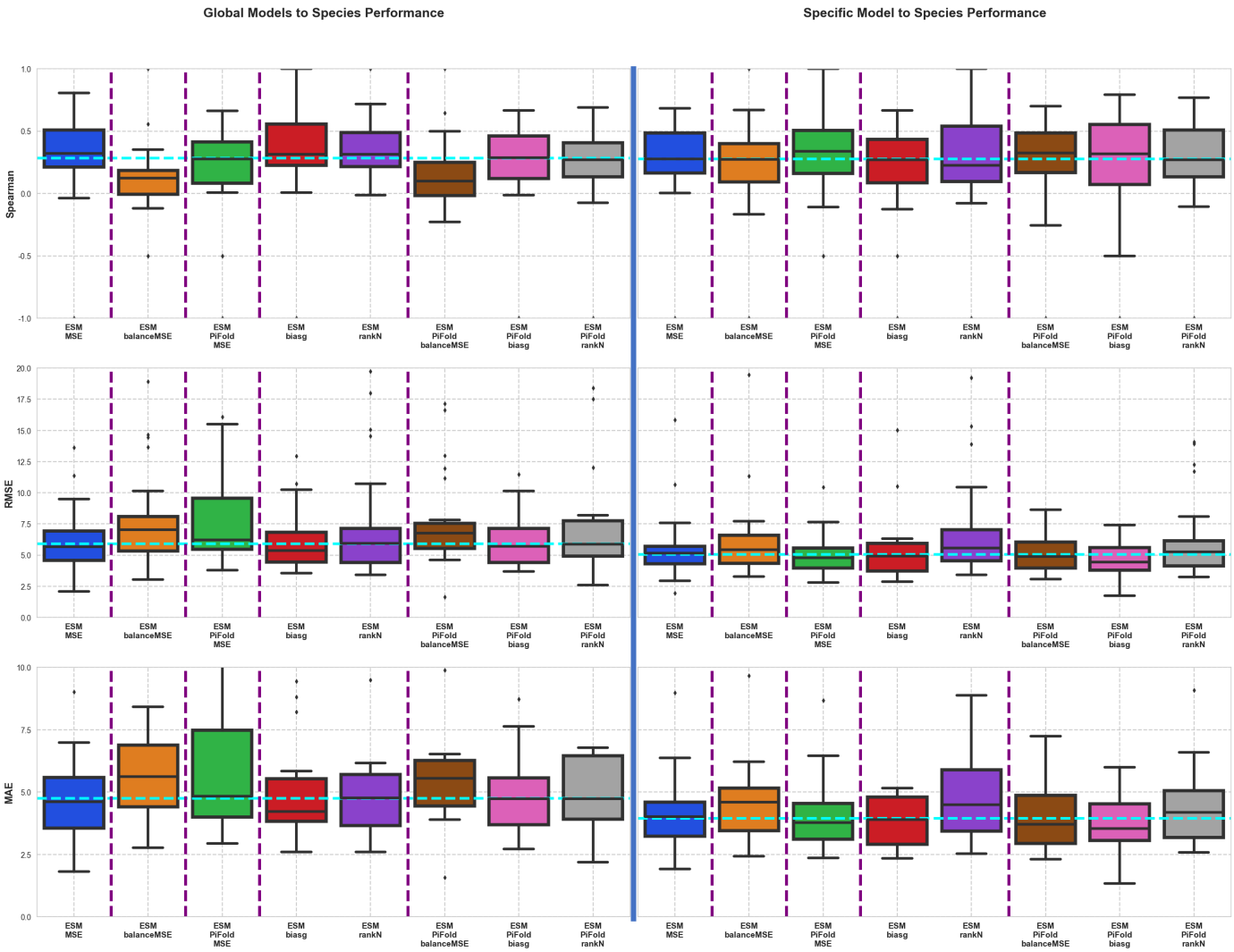

Figure 5: Box plots of the strategies used to predict thermostability. The blue line separates the use of global models applied to each species (right side) from the use of individual models for each species (left side). In addition, each region has subdivisions marked in purple, indicating the order in which the ideas were first tested: First, the prediction method using sequence embeddings was implemented. Next, species-by-species sampling was used in batches. Then the combination of sequence embeddings with inverse folding was used. Next, contrastive methods using sequence embeddings alone were applied. Finally, sequence embeddings were combined with contrastive methods. The cyan line crossing the box plots represents the average of the medians of all box plots. The points at the top and bottom of the box plots correspond to the outliers present in the predictions. Compared to the Boxplot shown in the main paper, this presents the boxplots related to all the performance metrics considered along the work, including: Spearman Correlation, RMSE and MAE respectively.

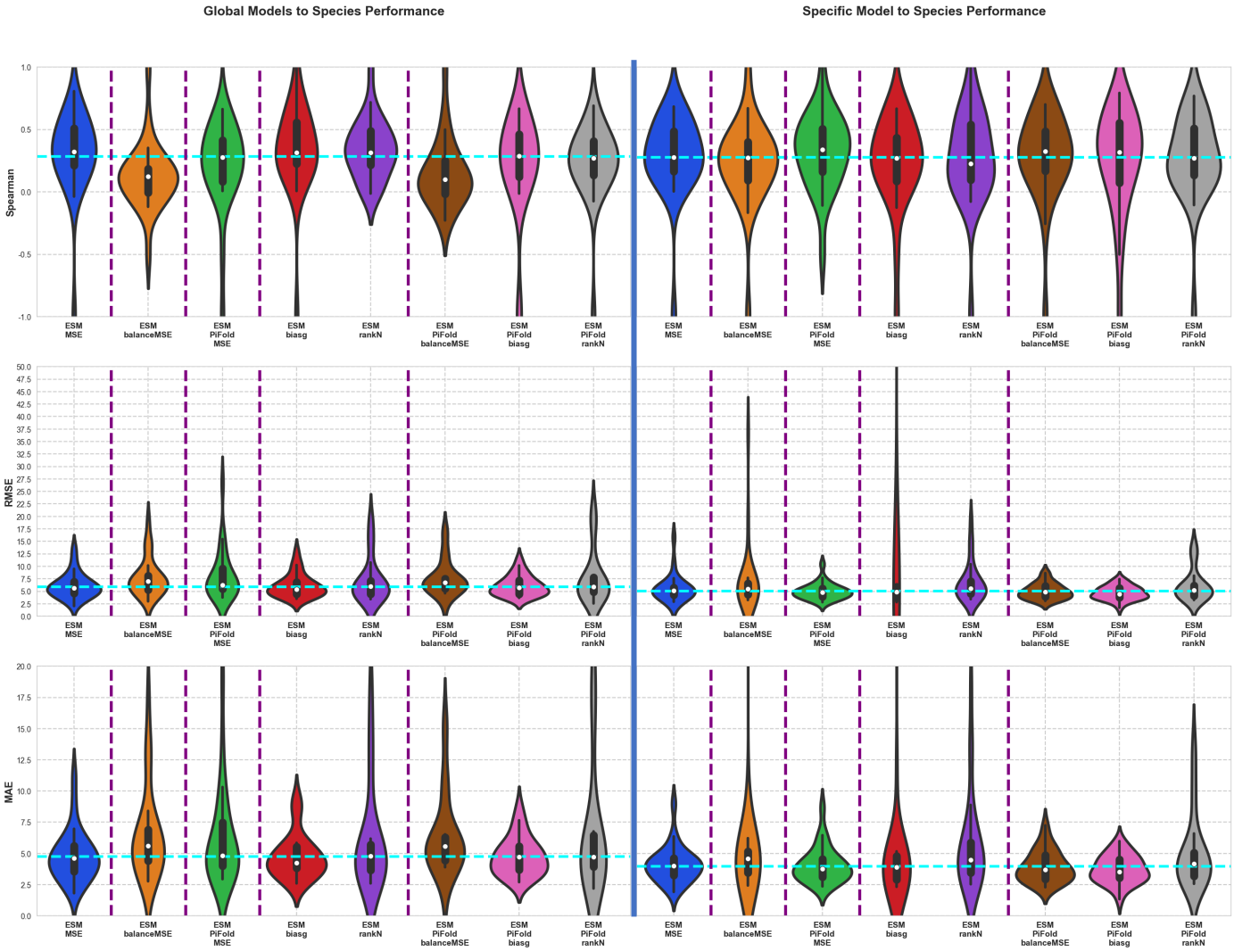

Figure 6: Violin plots of the strategies used to predict thermostability. The blue line separates the use of global models applied to each species (right side) from the use of individual models for each species (left side). In addition, each region has subdivisions marked in purple, indicating the order in which the ideas were first tested: First, the prediction method using sequence embeddings was implemented. Next, species-by-species sampling was used in batches. Then the combination of sequence embeddings with inverse folding was used. Next, contrastive methods using sequence embeddings alone were applied. Finally, sequence embeddings were combined with contrastive methods. The cyan line crossing the box plots represents the average of the medians of all violin plots. This plot show the variance and density estimation to all the performance metrics considered along the work, including: Spearman Correlation, RMSE and MAE respectively.

B Tables of Results for the Full Flip Split

Methods	global			
	Spearman	MSE	RMSE	MAE
MSE	0.688	37.303	6.1076	4.5268
balanceMSE	0.415	61.8778	7.8662	6.0651
biasg	0.6951	37.8031	6.1484	4.492
rank_l2_l1_MSE_001_t2	0.6356	53.1513	7.2905	5.3756

Table 3: Results of methods using sequence-based embeddings (ESM2). Performance evaluation using the full dataset of FLIP splits related to thermostability.

Methods	global			
	Spearman	MSE	RMSE	MAE
MSE	0.3763	87.9824	9.3799	6.788
balanceMSE	0.3563	100.758	10.0378	7.1735
biasg	0.3961	88.4589	9.4053	6.6275
rank_l2_l1_MSE_001_t2	0.309	98.5775	9.9286	7.0107

Table 4: Results of methods using embeddings from protein structures using Inverse Folding Algorithms (PiFold). Performance evaluation using the full dataset of FLIP splits related to thermostability.

Methods	global			
	Spearman	MSE	RMSE	MAE
MSE	0.679	42.8623	6.5469	4.7677
balanceMSE	0.5018	52.7803	7.265	5.676
biasg	0.6912	36.452	6.0376	4.481
rank_l2_l1_MSE_001_t2	0.6219	65.2838	8.0798	5.7973

Table 5: Results of methods using the concatenation of embeddings from ESM2 and PiFold. Performance evaluation using the full dataset of FLIP splits related to thermostability.

C Tables of Results for Global Models Applied to Individual Species

Methods	balanceMSE				biasg			
	Spearman	MSE	RMSE	MAE	Spearman	MSE	RMSE	MAE
Arabidopsis_thaliana_seedling_lysate	-0.0988	56.3553	7.507	5.9166	0.1737	40.3051	6.3486	4.6455
Bacillus_subtilis_168_lysate_R1	-0.1196	102.93	10.1454	8.4139	0.0487	65.4492	8.0901	5.8427
Caenorhabditis_elegans_lysate	0.1683	61.1264	7.8183	6.6306	0.2485	28.5346	5.3418	4.4649
Danio_rerio_Zenodo_lysate	0.0818	84.3226	9.1827	8.0521	0.7636	48.2345	6.9451	5.6205
Drosophila_melanogaster_SII_lysate	0.0362	49.3716	7.0265	5.8863	0.3217	14.5884	3.8195	3.0671
Ecoli_Lysate	0.1727	51.7253	7.192	5.8725	0.2293	53.0866	7.2861	5.7959
Escherichia_coli_cells	0.5557	51.5221	7.1779	6.3236	0.4178	104.673	10.231	8.8138
Geobacillus_stearothermophilus_NCA26_lysate	0.3519	186.93	13.6722	12.2979	0.2649	167.706	12.9501	9.4482
HAOEC	0.0601	49.3427	7.0244	5.1104	0.5448	34.5538	5.8782	4.3843
HEK293T	0.0989	21.5179	4.6387	3.5816	0.5893	14.4708	3.804	2.9393
HL60	0.2614	15.497	3.9366	3.0002	0.5686	16.5823	4.0721	2.725
HaCaT	0.1179	39.1102	6.2538	4.7219	0.5411	28.7117	5.3583	4.04
HepG2	-0.0364	42.8814	6.5484	5.2415	0.6338	25.9643	5.0955	3.9699
Jurkat	0.2568	27.7194	5.2649	4.383	0.562	19.2444	4.3868	3.6055
K562	1	9.2415	3.04	2.7739	-1	21.4709	4.6337	3.8368
Mus_musculus_BMDC_lysate	-0.0792	18.0147	4.2444	3.1469	0.2714	19.0719	4.3671	2.96
Mus_musculus_liver_lysate	0.1486	44.4799	6.6693	5.3624	0.1226	41.9219	6.4747	5.245
Oleispira_antarctica_RB-8_lysate_R1	0.1053	67.0532	8.1886	6.9769	0.2248	21.8788	4.6775	3.9502
Picrophilus_torridus_DSM9790_lysate	0.1438	208.776	14.4491	13.3615	0.2341	81.201	9.0112	5.7109
Saccharomyces_cerevisiae_lysate	0.1898	21.3975	4.6257	3.5893	0.3053	26.9074	5.1872	3.9288
Thermus_thermophilus_HB27_cells	0.1255	357.955	18.9197	17.3433	0.2166	115.26	10.7359	8.2072
Thermus_thermophilus_HB27_lysate	0.3065	214.4	14.6424	13.2952	0.3608	41.2089	6.4194	5.1294
U937	-0.0889	32.4743	5.6986	4.4815	0.6765	12.6116	3.5513	2.6062
colon_cancer_spheroids	-0.0208	24.8119	4.9812	3.9806	0.0078	23.8056	4.8791	3.8172
pTcells	-0.5	29.8796	5.4662	4.889	1	17.0161	4.1251	4.0651
MEANS	0.1295	74.7534	7.77256	6.5853	0.333108	43.3783	6.14678	4.75278

Methods	MSE				rankN			
	Spearman	MSE	RMSE	MAE	Spearman	MSE	RMSE	MAE
Arabidopsis_thaliana_seedling_lysate	0.1713	41.6821	6.4562	4.8311	0.0795	42.2389	6.4991	4.9576
Bacillus_subtilis_168_lysate_R1	0.0586	66.5909	8.1603	6.0094	-0.012	54.0174	7.3496	5.681
Caenorhabditis_elegans_lysate	0.34	31.8574	5.6442	4.7308	0.2828	43.6121	6.6039	5.7153
Danio_rerio_Zenodo_lysate	0.3636	49.33	7.0235	5.6581	0.7182	41.5056	6.4425	4.9886
Drosophila_melanogaster_SII_lysate	0.287	22.8456	4.7797	3.9267	0.2742	28.5485	5.3431	4.566
Ecoli_Lysate	0.2485	43.9449	6.6291	5.3792	0.2318	45.1501	6.7194	5.314
Escherichia_coli_cells	0.4553	71.6161	8.4626	6.9848	0.418	115.169	10.7317	9.4907
Geobacillus_stearothermophilus_NCA26_lysate	0.304	185.641	13.625	11.2403	0.3045	390.007	19.7486	18.7062
HAOEC	0.5905	28.7833	5.365	3.963	0.5018	33.2474	5.7661	4.2156
HEK293T	0.5569	12.9611	3.6001	2.818	0.4592	14.6691	3.83	3.0526
HL60	0.6305	13.4951	3.6736	2.5821	0.591	11.7356	3.4257	2.5935
HaCaT	0.5127	27.3408	5.2288	4.1923	0.378	31.8441	5.6431	4.5837
HepG2	0.6174	21.9505	4.6851	3.8385	0.5724	25.8588	5.0852	4.028
Jurkat	0.611	17.6694	4.2035	3.409	0.5221	19.1855	4.3801	3.6597
K562	-1	33.9431	5.8261	4.5849	1	15.6871	3.9607	3.8239
Mus_musculus_BMDC_lysate	0.264	18.5152	4.3029	3.0061	0.2366	13.5068	3.6752	2.6633
Mus_musculus_liver_lysate	0.0522	38.733	6.2236	5.0271	-0.0144	39.0666	6.2503	5.151
Oleispira_antarctica_RB-8_lysate_R1	0.2023	32.1654	5.6715	4.637	0.2087	37.8013	6.1483	5.2765
Picrophilus_torridus_DSM9790_lysate	0.1184	89.9399	9.4837	6.5683	0.0982	211.472	14.5421	12.2113
Saccharomyces_cerevisiae_lysate	0.3373	20.797	4.5604	3.4606	0.3222	20.4986	4.5275	3.4832
Thermus_thermophilus_HB27_cells	0.2481	129.526	11.3809	9.0225	0.1148	323.852	17.9959	16.0593
Thermus_thermophilus_HB27_lysate	0.3968	50.3902	7.0986	5.839	0.3073	226.428	15.0475	13.5913
U937	0.8059	9.5045	3.0829	2.3054	0.3971	17.5221	4.1859	3.3232
colon_cancer_spheroids	-0.0378	24.876	4.9876	3.8913	0.0026	20.7494	4.5552	3.6538
pTcells	0.5	4.3833	2.0936	1.8125	0.5	11.8894	3.4481	3.4415
MEANS	0.30538	43.5393	6.08994	4.78872	0.339784	73.4105	7.27619	6.16923

Table 6: Evaluation of methods using sequence-based embeddings (ESM2): Performance evaluation was performed using the full training and validation sets of FLIP partitions related to thermostability to induce the model. Testing was performed on individual species within the FLIP test set. The table shows the evaluation based on four primary metrics: Spearman correlation, MSE, RMSE and MAE, for the four methods analysed in this study (balanceMSE, biasg, MSE and RankN).

Methods	balanceMSE				biasg			
	Spearman	MSE	RMSE	MAE	Spearman	MSE	RMSE	MAE
Arabidopsis_thaliana_seedling_lysate	0.1978	43.6081	6.6036	5.1771	0.0682	47.5744	6.8974	5.3945
Bacillus_subtilis_168_lysate_R1	0.1186	64.2171	8.0136	6.2432	0.1013	90.2633	9.5007	7.0436
Caenorhabditis_elegans_lysate	0.1135	77.9945	8.8314	7.4103	0.1488	67.6063	8.2223	6.8556
Danio_rerio_Zenodo_lysate	0.1545	67.2587	8.2011	5.6998	0.4818	85.5648	9.2501	7.8557
Drosophila_melanogaster_SII_lysate	0.1883	42.6002	6.5269	5.436	0.0446	51.1427	7.1514	5.9902
Ecoli_Lysate	0.0712	61.3955	7.8355	6.194	0.101	72.936	8.5403	6.6497
Escherichia_coli_cells	0.2221	135.125	11.6243	10.0279	0.0373	176.004	13.2666	11.8437
Geobacillus_stearothermophilus_NCA26_lysate	0.088	498.251	22.3215	21.2174	0.0049	478.348	21.8712	19.6788
HAOEC	0.3888	49.0695	7.005	5.4388	0.3905	41.4828	6.4407	4.8899
HEK293T	0.3737	24.4279	4.9425	3.768	0.3315	21.264	4.6113	3.5963
HL60	0.2711	23.8911	4.8879	3.6236	0.3725	17.2556	4.154	3.2397
HaCaT	0.2216	45.1755	6.7213	4.7603	0.242	37.8045	6.1485	4.8963
HepG2	0.3273	38.7255	6.223	4.6599	0.4269	34.835	5.9021	4.8028
Jurkat	0.1976	34.0146	5.8322	4.6808	0.4273	25.7759	5.077	4.1718
K562	-1	4.0299	2.0075	1.5151	-1	18.3807	4.2873	4.287
Mus_musculus_BMDC_lysate	0.1254	26.6945	5.1667	3.6526	0.1506	27.9881	5.2904	3.6731
Mus_musculus_liver_lysate	0.1326	46.4017	6.8119	5.5285	0.1947	46.4456	6.8151	5.6925
Oleispira_antarctica_RB-8_lysate_R1	0.1121	59.6047	7.7204	6.3074	0.0632	61.3767	7.8343	6.0074
Picrophilus_torridus_DSM9790_lysate	-0.041	410.771	20.2675	18.9768	0.126	305.723	17.4849	14.515
Saccharomyces_cerevisiae_lysate	0.053	32.4263	5.6944	4.5244	0.3205	29.4371	5.4256	4.2492
Thermus_thermophilus_HB27_cells	-0.1055	838.375	28.9547	26.1275	-0.0737	642.825	25.354	20.9251
Thermus_thermophilus_HB27_lysate	0.0468	582.313	24.1312	21.609	-0.0441	483.995	21.9999	17.1478
U937	0.3706	25.0477	5.0048	4.2869	0.1	30.4037	5.514	4.1933
colon_cancer_spheroids	0.0613	26.1402	5.1127	4.1275	0.2479	38.4994	6.2048	4.5201
pTcells	0.5	34.794	5.8986	5.8971	-0.5	50.3598	7.0965	6.875
MEANS	0.127576	131.694	9.29361	7.8756	0.110548	119.332	9.21362	7.55976

Methods	MSE				rankN			
	Spearman	MSE	RMSE	MAE	Spearman	MSE	RMSE	MAE
Arabidopsis_thaliana_seedling_lysate	0.0615	49.9119	7.0648	5.4569	0.04	47.601	6.8993	5.3863
Bacillus_subtilis_168_lysate_R1	0.0577	77.1768	8.785	6.8443	-0.0649	67.5899	8.2213	6.6734
Caenorhabditis_elegans_lysate	0.2483	88.5995	9.4127	8.0938	-0.0366	76.9103	8.7699	7.6532
Danio_rerio_Zenodo_lysate	-0.0182	63.064	7.9413	5.9462	0.6545	53.9727	7.3466	5.702
Drosophila_melanogaster_SII_lysate	0.2405	56.1757	7.495	6.493	0.3073	40.6112	6.3727	5.6224
Ecoli_Lysate	0.0873	66.5738	8.1593	6.4321	-0.0549	59.2102	7.6948	6.0148
Escherichia_coli_cells	0.0935	141.508	11.8957	10.15	0.0313	108.28	10.4057	9.1288
Geobacillus_stearothermophilus_NCA26_lysate	-0.0762	402.561	20.0639	18.2502	-0.2718	397.585	19.9395	18.0143
HAOEC	0.389	37.326	6.1095	4.579	0.3736	47.5098	6.8927	5.0855
HEK293T	0.3936	23.1623	4.8127	3.5236	0.3369	23.2582	4.8227	3.5999
HL60	0.3305	19.1996	4.3817	3.4348	0.354	19.2183	4.3839	3.1957
HaCaT	0.0785	40.7701	6.3851	5.359	0.3414	39.0351	6.2478	4.8033
HepG2	0.5175	25.7657	5.076	4.0447	0.4026	34.4372	5.8683	4.7732
Jurkat	0.5916	17.522	4.1859	3.4371	0.2134	31.7117	5.6313	4.5822
K562	1	5.6946	2.3863	2.1568	0	5.059	2.2492	1.8709
Mus_musculus_BMDC_lysate	0.21	20.926	4.5745	3.4033	0.1203	16.1929	4.024	2.9002
Mus_musculus_liver_lysate	-0.0108	46.809	6.8417	5.7137	-0.0597	48.1737	6.9407	5.7201
Oleispira_antarctica_RB-8_lysate_R1	0.0712	74.8146	8.6495	7.3418	0.1333	72.2167	8.498	7.3424
Picrophilus_torridus_DSM9790_lysate	0.1537	314.616	17.7374	15.7521	-0.0237	393.507	19.837	18.6257
Saccharomyces_cerevisiae_lysate	0.1838	21.5273	4.6398	3.6465	0.1058	21.5062	4.6375	3.6898
Thermus_thermophilus_HB27_cells	-0.1581	815.522	28.5573	25.5008	-0.013	860.323	29.3313	26.241
Thermus_thermophilus_HB27_lysate	0.0875	492.982	22.2032	19.2164	0.0335	609.46	24.6873	22.0347
U937	0.4765	22.0209	4.6926	3.7639	0.3316	28.9023	5.3761	4.2117
colon_cancer_spheroids	0.3813	23.1553	4.812	3.6682	0.27	18.2909	4.2768	3.5334
pTcells	0.5	46.0152	6.7835	6.4249	-0.5	36.0084	6.0007	5.9248
MEANS	0.235608	119.736	8.94586	7.54532	0.120996	126.263	9.0142	7.69319

Table 7: Evaluation of methods using embeddings from protein structures via inverse folding (PiFold): Performance evaluation was performed using the full training and validation sets of FLIP partitions related to thermostability to induce the model. Testing was performed on individual species within the FLIP test set. The table shows the evaluation based on four primary metrics: Spearman correlation, MSE, RMSE and MAE, for the four methods analysed in this study (balanceMSE, biasg, MSE and RankN).

Methods	balanceMSE				biasg			
	Spearman	MSE	RMSE	MAE	Spearman	MSE	RMSE	MAE
Arabidopsis_thaliana_seedling_lysate	-0.0328	44.9936	6.7077	5.1725	0.1137	42.7874	6.5412	5.0204
Bacillus_subtilis_168_lysate_R1	0.0251	48.0577	6.9324	5.6365	-0.0123	75.4061	8.6837	6.5255
Caenorhabditis_elegans_lysate	0.1034	45.9781	6.7807	5.8325	0.3285	32.324	5.6854	4.6984
Danio_rerio_Zenodo_lysate	0.6455	61.3115	7.8302	6.5264	0.6455	46.4755	6.8173	5.611
Drosophila_melanogaster_SII_lysate	0.1124	25.6896	5.0685	4.1189	0.3215	20.6017	4.5389	3.6341
Ecoli_Lysate	0.0858	50.1222	7.0797	5.7697	0.2931	43.929	6.6279	5.4187
Escherichia_coli_cells	0.3961	124.554	11.1604	9.8918	0.3531	72.1184	8.4923	7.3403
Geobacillus_stearothermophilus_NCA26_lysate	0.2636	293.461	17.1307	15.6566	0.2785	131.69	11.4756	8.7325
HAOEC	-0.0117	52.6367	7.2551	5.5859	0.5974	28.9445	5.38	3.9445
HEK293T	-0.0166	30.0877	5.4852	4.3884	0.4751	16.0743	4.0093	3.0436
HL60	-0.026	27.6587	5.2592	4.0565	0.5124	13.6517	3.6948	2.713
HaCaT	-0.2289	55.3317	7.4385	5.8553	0.6654	24.5686	4.9567	4.0428
HepG2	-0.0209	47.0074	6.8562	5.5277	0.5767	23.547	4.8525	3.8697
Jurkat	-0.2288	45.9317	6.7773	5.9716	0.5776	16.0434	4.0054	3.3378
K562	1	2.7174	1.6485	1.5705	-1	55.7615	7.4674	5.3456
Mus_musculus_BMDC_lysate	-0.0049	23.717	4.87	3.8992	0.2541	18.3161	4.2797	2.9783
Mus_musculus_liver_lysate	0.1471	43.8143	6.6192	5.4036	0.1062	38.0584	6.1692	4.8434
Oleispira_antarctica_RB-8_lysate_R1	0.1304	32.0531	5.6616	4.8655	0.1592	32.9704	5.742	4.7691
Picrophilus_torridus_DSM9790_lysate	0.0946	168.576	12.9837	10.7069	-0.0145	80.3387	8.9632	6.2426
Saccharomyces_cerevisiae_lysate	0.0423	30.4126	5.5148	4.3921	0.3267	18.9499	4.3531	3.2769
Thermus_thermophilus_HB27_cells	0.2346	276.846	16.6387	14.5587	0.1349	102.891	10.1435	7.6395
Thermus_thermophilus_HB27_lysate	0.3538	143.249	11.9687	10.2945	0.2823	52.6987	7.2594	5.6441
U937	0.2529	33.3963	5.779	4.7876	0.4147	14.9665	3.8687	3.0603
colon_cancer_spheroids	-0.1639	31.1899	5.5848	4.6067	0.0389	24.9092	4.9909	3.8851
pTcells	0.5	21.1659	4.6006	4.2683	-1	19.0944	4.3697	3.8958
MEANS	0.146124	70.3984	7.58526	6.37376	0.217148	41.8846	6.13471	4.78052

Methods	MSE				rankN			
	Spearman	MSE	RMSE	MAE	Spearman	MSE	RMSE	MAE
Arabidopsis_thaliana_seedling_lysate	0.109	39.2262	6.2631	4.8214	0.1274	36.2154	6.0179	4.5516
Bacillus_subtilis_168_lysate_R1	0.0245	59.9784	7.7446	5.7714	0.0426	37.9457	6.16	4.8815
Caenorhabditis_elegans_lysate	0.3299	32.1148	5.667	4.8481	0.2677	33.5518	5.7924	4.8652
Danio_rerio_Zenodo_lysate	0.6636	47.1145	6.864	5.3625	0.6909	67.0075	8.1858	6.6925
Drosophila_melanogaster_SII_lysate	0.2991	22.454	4.7386	3.8411	0.381	17.4374	4.1758	3.4377
Ecoli_Lysate	0.2094	47.4049	6.8851	5.5404	0.2948	52.1178	7.2193	5.7509
Escherichia_coli_cells	0.3589	99.9341	9.9967	8.4899	0.2228	144.307	12.0128	10.624
Geobacillus_stearothermophilus_NCA26_lysate	0.2144	258.657	16.0828	13.9394	0.271	464.474	21.5517	20.7134
HAOEC	0.5121	32.7875	5.726	4.1267	0.4289	45.9515	6.7788	5.0711
HEK293T	0.4918	14.5158	3.81	2.9418	0.3636	18.5763	4.31	3.312
HL60	0.5576	25.8021	5.0796	3.0008	0.4153	15.7443	3.9679	2.8836
HaCaT	0.4221	29.4583	5.4275	4.4413	0.2096	35.3295	5.9439	4.6046
HepG2	0.5828	31.2366	5.589	4.0038	0.5321	31.8896	5.6471	4.3951
Jurkat	0.5608	34.4767	5.8717	4.0023	0.426	25.9512	5.0942	4.2632
K562	-1	714.098	26.7226	19.1323	-1	6.7103	2.5904	2.1838
Mus_musculus_BMDC_lysate	0.266	16.9931	4.1223	3.0564	0.2084	14.4295	3.7986	2.7389
Mus_musculus_liver_lysate	0.0062	40.8254	6.3895	5.0758	0.0941	48.9111	6.9936	5.7595
Oleispira_antarctica_RB-8_lysate_R1	0.1337	24.9606	4.9961	4.1284	0.1489	27.9463	5.2864	4.5097
Picrophilus_torridus_DSM9790_lysate	0.0185	119.918	10.9507	8.2336	0.0208	338.396	18.3955	16.5375
Saccharomyces_cerevisiae_lysate	0.3261	20.3761	4.514	3.4657	0.2844	27.5199	5.2459	4.2572
Thermus_thermophilus_HB27_cells	0.073	170.008	13.0387	10.0611	0.0676	431.125	20.7636	18.904
Thermus_thermophilus_HB27_lysate	0.2913	120.471	10.9759	7.906	0.2938	307.381	17.5323	16.1797
U937	0.3941	38.377	6.1949	3.9725	0.6	19.7639	4.4457	3.4367
colon_cancer_spheroids	0.0681	33.1918	5.7612	4.0455	-0.0761	23.4299	4.8404	3.8038
pTcells	-0.5	239.848	15.487	10.3164	0.5	27.3404	5.2288	5.0902
MEANS	0.21652	92.5691	8.19594	6.18098	0.232624	91.9781	7.91915	6.7779

Table 8: Evaluation of methods using concatenation of embeddings from ESM2 and PiFold: Performance evaluation was performed using the full training and validation sets of FLIP partitions related to thermostability to induce the model. Testing was performed on individual species within the FLIP test set. The table shows the evaluation based on four primary metrics: Spearman correlation, MSE, RMSE and MAE, for the four methods analysed in this study (balanceMSE, biasg, MSE and RankN).

D Tables of Results for Individual Model per Species

Methods	balanceMSE				biasg			
	Spearman	MSE	RMSE	MAE	Spearman	MSE	RMSE	MAE
Arabidopsis_thaliana_seedling_lysate	0.2852	35.1803	5.9313	4.571	0.3915	28.9075	5.3766	4.0307
Bacillus_subtilis_168_lysate_R1	0.2912	24.1663	4.9159	3.7388	0.3267	23.8897	4.8877	3.8329
Caenorhabditis_elegans_lysate	0.3766	379.356	19.4771	4.6509	0.45	21.898	4.6795	3.5624
Danio_rerio_Zenodo_lysate	0.0909	128.475	11.3347	9.6606	-0.1273	225.52	15.0173	12.0062
Drosophila_melanogaster_SII_lysate	0.1526	15.3985	3.9241	3.0623	0.2276	12.6765	3.5604	2.8362
Ecoli_Lysate	0.407	36.5361	6.0445	4.8506	0.4971	33.2729	5.7683	4.626
Escherichia_coli_cells	0.5233	45.1256	6.7176	5.6226	0.6143	28.6546	5.353	4.3872
Geobacillus_stearothermophilus_NCA26_lysate	0.0901	39.4851	6.2837	5.2636	0.0798	35.8998	5.9916	4.8417
HAOEC	0.6683	18.0296	4.2461	3.3848	0.6677	17.5784	4.1927	3.1416
HEK293T	0.3765	16.5299	4.0657	3.1876	0.6461	11.0681	3.3269	2.6517
HL60	0.4633	11.4203	3.3794	2.7111	0.6226	9.6282	3.1029	2.5825
HaCaT	0.2289	44.3847	6.6622	4.8588	0.2811	39.1072	6.2536	4.9183
HepG2	0.428	31.5882	5.6203	4.3371	0.05	39.9588	6.3213	5.1588
Jurkat	0.4148	24.0002	4.899	3.8913	0.3752	24.4667	4.9464	4.2259
K562	-1	23.8188	4.8804	4.6064	-1	8.9454	2.9909	2.624
Mus_musculus_BMDC_lysate	0.3239	10.8574	3.2951	2.4241	0.3697	10.7146	3.2733	2.3409
Mus_musculus_liver_lysate	-0.1671	36.438	6.0364	4.8889	0.0819	32.2965	5.683	4.659
Oleispira_antarctica_RB-8_lysate_R1	0.0454	26.8454	5.1813	3.8702	0.0335	18.6379	4.3172	3.2358
Picrophilus_torridus_DSM9790_lysate	0.165	41.0108	6.404	4.9941	0.2599	24.9528	4.9953	3.9412
Saccharomyces_cerevisiae_lysate	0.2978	17.0026	4.1234	3.1669	0.3283	17.5996	4.1952	3.1873
Thermus_thermophilus_HB27_cells	0.0117	1354.8	36.8076	29.4928	0.1002	20153.3	141.962	25.2994
Thermus_thermophilus_HB27_lysate	0.1008	59.3835	7.7061	6.2203	0.2217	36.9322	6.0772	4.8796
U937	0.2618	18.036	4.2469	3.2158	0.6588	11.882	3.447	2.6935
colon_cancer_spheroids	-0.0616	21.4252	4.6287	3.6292	0.1363	17.5956	4.1947	3.4264
pTcells	1	27.8208	5.2745	5.2123	-0.5	8.1613	2.8568	2.5818
MEANS	0.230976	99.4846	7.28344	5.42048	0.231708	835.74	10.5108	4.86684

Methods	MSE				rankN			
	Spearman	MSE	RMSE	MAE	Spearman	MSE	RMSE	MAE
Arabidopsis_thaliana_seedling_lysate	0.2757	31.0004	5.5678	4.3043	0.1801	33.4706	5.7854	4.4929
Bacillus_subtilis_168_lysate_R1	0.2119	26.0025	5.0993	3.944	-0.0782	26.5269	5.1504	3.9686
Caenorhabditis_elegans_lysate	0.4443	251.104	15.8463	4.3104	0.4126	23.4481	4.8423	3.6256
Danio_rerio_Zenodo_lysate	0.1636	113.312	10.6448	8.979	0.4818	369.521	19.2229	18.4969
Drosophila_melanogaster_SII_lysate	0.3183	11.3899	3.3749	2.6573	0.1157	11.7702	3.4308	2.7413
Ecoli_Lysate	0.4357	35.479	5.9564	4.8229	0.4253	42.1144	6.4896	5.3407
Escherichia_coli_cells	0.5606	32.7802	5.7254	4.8546	0.3895	70.6396	8.4047	7.2346
Geobacillus_stearothermophilus_NCA26_lysate	0.2564	31.6178	5.623	4.5296	0.1179	34.9162	5.909	4.8523
HAOEC	0.6832	16.7097	4.0877	3.2149	0.6621	20.0385	4.4764	3.2012
HEK293T	0.5759	12.533	3.5402	2.7081	0.6298	12.7439	3.5699	2.8206
HL60	0.6247	8.6127	2.9347	2.4174	0.6328	12.4881	3.5338	2.8032
HaCaT	0.6781	23.5524	4.8531	3.6007	0.2961	81.834	9.0462	7.3093
HepG2	0.4166	27.5064	5.2447	4.198	0.7306	18.2769	4.2751	3.3763
Jurkat	0.5497	20.3893	4.5155	3.6091	0.56	26.8047	5.1773	4.1779
K562	-1	20.0878	4.4819	3.5169	-1	33.2189	5.7636	5.5281
Mus_musculus_BMDC_lysate	0.3265	10.8	3.2863	2.3875	0.0678	12.1015	3.4787	2.5353
Mus_musculus_liver_lysate	0.094	31.4523	5.6082	4.6244	0.0873	29.042	5.3891	4.4974
Oleispira_antarctica_RB-8_lysate_R1	0.0911	18.3544	4.2842	3.2036	-0.0215	109.501	10.4643	8.8855
Picrophilus_torridus_DSM9790_lysate	0.222	29.4879	5.4303	4.3721	0.0355	234.615	15.3172	13.448
Saccharomyces_cerevisiae_lysate	0.2468	18.84	4.3405	3.2997	0.1777	17.2934	4.1585	3.3133
Thermus_thermophilus_HB27_cells	0.1717	57.7222	7.5975	6.3657	0.1418	50.6287	7.1154	5.9142
Thermus_thermophilus_HB27_lysate	0.0034	50.3409	7.0951	5.8207	0.1577	38.7479	6.2248	5.1955
U937	0.0412	51.165	7.153	4.7931	0.5824	23.3845	4.8357	3.8638
colon_cancer_spheroids	0.1359	19.8405	4.4543	3.6356	-0.02	22.0879	4.6998	3.6528
pTcells	0.5	3.8066	1.9511	1.9092	1	193.474	13.9095	13.5656
MEANS	0.281092	38.1555	5.54785	4.08315	0.270592	61.9475	6.82682	5.79364

Table 9: Assessment of methodologies employing sequence-based embeddings from ESM2: The performance of individual models was assessed for each species and subsequently tested on that target species inside the FLIP partition. Spearman correlation, mean square error (MSE), root mean square error (RMSE) and mean absolute error (MAE). These metrics were used to analyse the effectiveness of the four methods investigated in this study: balanceMSE, biasg, MSE and RankN.

Methods	balanceMSE				biasg			
	Spearman	MSE	RMSE	MAE	Spearman	MSE	RMSE	MAE
Arabidopsis_thaliana_seedling_lysate	0.1901	33.1926	5.7613	4.416	0.2502	31.8047	5.6396	4.36
Bacillus_subtilis_168_lysate_R1	0.235	26.0891	5.1078	3.8833	0.2005	26.9053	5.187	4.0578
Caenorhabditis_elegans_lysate	0.2814	23.3374	4.8309	3.8388	0.2717	24.0761	4.9067	3.7928
Danio_rerio_Zenodo_lysate	0.0545	55.0791	7.4215	5.9855	-0.1909	85.0409	9.2218	6.6883
Drosophila_melanogaster_SII_lysate	0.332	11.2	3.3466	2.6635	0.2971	11.8738	3.4458	2.6509
Ecoli_Lysate	0.2438	49.9904	7.0704	5.551	0.3893	38.8821	6.2355	5.0328
Escherichia_coli_cells	0.2479	62.1012	7.8804	6.5516	0.1184	53.963	7.346	6.2021
Geobacillus_stearothermophilus_NCA26_lysate	0.0345	43.1849	6.5715	5.3951	0.0842	41.817	6.4666	5.1216
HAOEC	0.5553	21.1289	4.5966	3.6297	0.5702	21.5063	4.6375	3.5582
HEK293T	0.3274	18.916	4.3493	3.4813	0.3553	16.8959	4.1105	3.3724
HL60	0.5285	12.7037	3.5642	2.8803	0.5094	12.7012	3.5639	2.8331
HaCaT	0.0953	46.8168	6.8423	5.0379	0.0528	57.0223	7.5513	5.5844
HepG2	0.4819	27.8663	5.2789	4.0159	0.5148	25.9791	5.097	4.1233
Jurkat	0.3438	27.167	5.2122	4.2192	0.0998	29.5164	5.4329	4.4984
K562	-1	20.4271	4.5196	4.0903	-1	14.7407	3.8394	3.6112
Mus_musculus_BMDC_lysate	0.1828	12.4816	3.5329	2.5956	0.2007	12.7979	3.5774	2.5749
Mus_musculus_liver_lysate	0.1398	29.6782	5.4478	4.4864	0.1861	139.129	11.7953	5.8553
Oleispira_antarctica_RB-8_lysate_R1	-0.0207	24.0207	4.9011	3.762	0.0777	17.7828	4.217	3.183
Picrophilus_torridus_DSM9790_lysate	0.0646	37.0564	6.0874	4.8446	0.113	28.2721	5.3171	4.3029
Saccharomyces_cerevisiae_lysate	0.0481	19.6548	4.4334	3.4708	0.1198	18.515	4.3029	3.395
Thermus_thermophilus_HB27_cells	-0.0552	73.09	8.5493	7.1818	-0.0566	63.1341	7.9457	6.5063
Thermus_thermophilus_HB27_lysate	0.0847	45.8389	6.7704	5.6529	0.1028	41.072	6.4087	5.3268
U937	0.5971	15.4958	3.9365	2.7684	0.1588	17.6512	4.2013	3.4349
colon_cancer_spheroids	0.1604	17.373	4.1681	3.4119	0.0388	19.2596	4.3886	3.5495
pTcells	0.5	26.5078	5.1486	4.3754	0.5	8.3234	2.885	2.6848
MEANS	0.18612	31.2159	5.41316	4.32757	0.158556	34.3465	5.50882	4.25203

Methods	MSE				rankN			
	Spearman	MSE	RMSE	MAE	Spearman	MSE	RMSE	MAE
Arabidopsis_thaliana_seedling_lysate	0.1513	33.8696	5.8198	4.4579	0.1197	32.8702	5.7332	4.5013
Bacillus_subtilis_168_lysate_R1	0.1527	28.1217	5.303	4.1673	0.147	26.1166	5.1104	4.0038
Caenorhabditis_elegans_lysate	0.3198	24.1727	4.9166	3.7621	0.1201	25.0226	5.0023	3.9697
Danio_rerio_Zenodo_lysate	0.6	33.9685	5.8282	4.6552	0.1545	39.9804	6.323	4.7511
Drosophila_melanogaster_SII_lysate	0.3204	10.97	3.3121	2.5842	0.3396	12.9318	3.5961	2.8986
Ecoli_Lysate	0.2583	42.3656	6.5089	5.2799	0.4019	48.3124	6.9507	5.6156
Escherichia_coli_cells	0.367	58.9055	7.675	6.5599	-0.0351	61.2983	7.8293	6.7248
Geobacillus_stearothermophilus_NCA26_lysate	-0.106	39.5683	6.2903	4.9254	0.1681	33.9255	5.8246	4.5943
HAOEC	0.6131	19.766	4.4459	3.5534	0.5151	24.2065	4.92	3.6582
HEK293T	0.5067	14.7227	3.837	3.0679	0.4558	14.4314	3.7989	2.998
HL60	0.5877	9.8337	3.1359	2.5131	0.1545	16.2364	4.0294	3.0754
HaCaT	0.4174	34.1148	5.8408	4.4338	0.3616	36.3923	6.0326	4.6482
HepG2	0.6413	19.7246	4.4412	3.4868	0.5916	23.1588	4.8124	3.8102
Jurkat	0.3163	26.6553	5.1629	4.2983	0.271	24.4258	4.9422	4.2085
K562	1	27.3812	5.2327	5.1922	-1	5.3537	2.3138	1.9069
Mus_musculus_BMDC_lysate	0.2036	12.4449	3.5277	2.4947	0.1087	11.8251	3.4388	2.535
Mus_musculus_liver_lysate	0.2019	26.4774	5.1456	4.1962	-0.0673	30.653	5.5365	4.6092
Oleispira_antarctica_RB-8_lysate_R1	0.0616	18.4959	4.3007	3.3799	0.1153	16.5094	4.0632	3.0985
Picrophilus_torridus_DSM9790_lysate	0.0001	31.7089	5.6311	4.547	0.2134	31.4108	5.6045	4.391
Saccharomyces_cerevisiae_lysate	0.2475	17.3746	4.1683	3.1798	0.2441	23.5091	4.8486	3.9765
Thermus_thermophilus_HB27_cells	-0.015	58.7667	7.6659	6.0328	-0.057	48.9728	6.9981	5.7465
Thermus_thermophilus_HB27_lysate	0.0471	49.1931	7.0138	5.7324	0.1022	37.4915	6.123	5.083
U937	-0.1235	24.0018	4.8992	3.9386	-0.1324	18.1745	4.2632	3.5649
colon_cancer_spheroids	0.0761	18.1357	4.2586	3.4174	0.0622	17.8032	4.2194	3.4283
pTcells	0.5	26.305	5.1288	4.9994	-0.5	18.0692	4.2508	3.7284
MEANS	0.293816	28.2818	5.1796	4.19422	0.114184	27.1633	5.0626	4.06104

Table 10: Assessment of methodologies employing embeddings from protein structures using Inverse Folding algorithms (PiFold): The performance of individual models was assessed for each species and subsequently tested on that target species inside the FLIP partition. Spearman correlation, mean square error (MSE), root mean square error (RMSE) and mean absolute error (MAE). These metrics were used to analyse the effectiveness of the four methods investigated in this study: balanceMSE, biasg, MSE and RankN.

Methods	balanceMSE				biasg			
	Spearman	MSE	RMSE	MAE	Spearman	MSE	RMSE	MAE
Arabidopsis_thaliana_seedling_lysate	0.3505	29.5605	5.437	4.1579	0.3321	30.1566	5.4915	4.1206
Bacillus_subtilis_168_lysate_R1	0.2232	25.9268	5.0918	3.901	0.3015	26.9116	5.1876	4.2273
Caenorhabditis_elegans_lysate	0.368	22.4169	4.7346	3.6779	0.4724	20.5988	4.5386	3.5272
Danio_rerio_Zenodo_lysate	-0.2545	72.4703	8.5129	6.3495	0.3364	48.9019	6.993	5.3776
Drosophila_melanogaster_SII_lysate	0.3374	10.9702	3.3121	2.6325	0.4173	10.1633	3.188	2.5342
Ecoli_Lysate	0.382	40.7093	6.3804	5.0832	0.5134	31.3316	5.5975	4.5145
Escherichia_coli_cells	0.5293	44.9233	6.7025	5.6516	0.5683	34.6805	5.889	4.8422
Geobacillus_stearothermophilus_NCA26_lysate	0.1632	39.2467	6.2647	5.0332	0.2924	31.5223	5.6145	4.5322
HAOEC	0.6825	16.6991	4.0865	2.9802	0.6785	16.2852	4.0355	3.166
HEK293T	0.6503	10.8033	3.2868	2.6429	0.5679	12.6298	3.5538	2.8093
HL60	0.663	9.4643	3.0764	2.4607	0.663	9.4511	3.0743	2.5043
HaCaT	-0.0057	47.7258	6.9084	5.1539	-0.3245	48.5773	6.9697	5.5694
HepG2	0.6987	16.7001	4.0866	3.242	0.7914	14.4484	3.8011	3.0977
Jurkat	0.444	23.4916	4.8468	3.7271	0.6486	16.1099	4.0137	3.2487
K562	-1	11.0728	3.3276	2.8619	-1	3.0531	1.7473	1.3394
Mus_musculus_BMDC_lysate	0.3702	10.9503	3.3091	2.3	0.286	11.6081	3.4071	2.3945
Mus_musculus_liver_lysate	0.2139	26.6532	5.1627	4.2005	-0.0108	31.4768	5.6104	4.6453
Oleispira_antarctica_RB-8_lysate_R1	0.035	24.5496	4.9548	3.5839	0.1266	16.7649	4.0945	3.0388
Picrophilus_torridus_DSM9790_lysate	0.2688	29.8296	5.4617	4.3719	0.0523	27.8212	5.2746	4.1684
Saccharomyces_cerevisiae_lysate	0.3152	15.6218	3.9524	3.1088	0.2702	16.1805	4.0225	3.0964
Thermus_thermophilus_HB27_cells	0.1111	74.9102	8.6551	7.2418	0.0171	55.0932	7.4225	5.989
Thermus_thermophilus_HB27_lysate	0.0642	45.6323	6.7552	5.4227	0.3609	38.8648	6.2342	5.0251
U937	0.6794	12.4133	3.5232	2.9262	0.6765	9.8029	3.131	2.6008
colon_cancer_spheroids	0.1879	16.9934	4.1223	3.4596	-0.1437	18.6022	4.313	3.4689
pTcells	0.5	15.8435	3.9804	2.8804	-0.5	14.422	3.7976	3.5517
MEANS	0.279104	27.8231	5.03728	3.96205	0.255752	23.8183	4.6801	3.73558

Methods	MSE				rankN			
	Spearman	MSE	RMSE	MAE	Spearman	MSE	RMSE	MAE
Arabidopsis_thaliana_seedling_lysate	0.3461	29.1147	5.3958	4.1742	0.1444	33.0563	5.7495	4.4886
Bacillus_subtilis_168_lysate_R1	0.1653	25.9705	5.0961	4.0067	0.1319	25.9661	5.0957	3.9435
Caenorhabditis_elegans_lysate	0.499	20.6519	4.5444	3.4613	0.4784	21.4948	4.6362	3.4993
Danio_rerio_Zenodo_lysate	0.0455	109.125	10.4463	8.6692	0.0364	193.913	13.9253	12.4161
Drosophila_melanogaster_SII_lysate	0.3202	12.096	3.4779	2.7011	0.3287	10.5318	3.2453	2.5795
Ecoli_Lysate	0.4779	31.9304	5.6507	4.5741	0.5269	33.6137	5.7977	4.6787
Escherichia_coli_cells	0.5883	31.4554	5.6085	4.7336	0.5132	65.2721	8.0791	6.593
Geobacillus_stearothermophilus_NCA26_lysate	0.1593	37.1683	6.0966	5.0318	0.0914	33.9548	5.8271	4.8257
HAOEC	0.6695	16.8059	4.0995	3.148	0.6921	18.7967	4.3355	3.1634
HEK293T	0.4082	15.5122	3.9386	3.1006	0.5787	12.4972	3.5351	2.6919
HL60	0.6704	7.8528	2.8023	2.3577	0.6633	12.8484	3.5845	2.8722
HaCaT	0.4248	26.0739	5.1063	4.0582	-0.1043	150.318	12.2604	9.0783
HepG2	0.6422	20.104	4.4837	3.5313	0.7702	18.014	4.2443	3.3321
Jurkat	0.558	18.3289	4.2812	3.419	0.6849	23.2359	4.8204	3.8469
K562	1	42.885	6.5487	6.3414	-1	25.5311	5.0528	4.0778
Mus_musculus_BMDC_lysate	0.3303	11.1626	3.3411	2.47	0.1396	12.6878	3.562	2.5788
Mus_musculus_liver_lysate	0.1039	28.9951	5.3847	4.4282	0.2819	30.818	5.5514	4.3435
Oleispira_antarctica_RB-8_lysate_R1	0.0069	19.2697	4.3897	3.3043	0.2918	15.99	3.9988	2.9648
Picrophilus_torridus_DSM9790_lysate	0.2891	26.4809	5.146	4.1468	0.1515	137.6	11.7303	10.1876
Saccharomyces_cerevisiae_lysate	0.3907	15.1299	3.8897	2.9698	0.2702	16.3817	4.0474	3.1665
Thermus_thermophilus_HB27_cells	0.1968	58.7222	7.663	6.4591	0.1177	47.7578	6.9107	5.6658
Thermus_thermophilus_HB27_lysate	-0.1086	45.6133	6.7538	5.5957	0.0697	35.6751	5.9729	4.9608
U937	0.5059	12.1784	3.4898	3.0624	0.1618	29.4041	5.4226	4.2814
colon_cancer_spheroids	0.0397	18.7022	4.3246	3.4427	0.189	16.633	4.0784	3.201
pTcells	-0.5	9.1506	3.025	2.8475	0.5	198.42	14.0862	13.8163
MEANS	0.329176	27.6192	4.99936	4.08139	0.268376	48.8165	6.22198	5.09014

Table 11: Assessment of methodologies using the combination of ESM2 and PiFold embeddings: The performance of individual models was assessed for each species and subsequently tested on that target species inside the FLIP partition. Spearman correlation, mean square error (MSE), root mean square error (RMSE) and mean absolute error (MAE). These metrics were used to analyse the effectiveness of the four methods investigated in this study: balanceMSE, biasg, MSE and RankN.

E Cross-species Prediction Scatterplots - Global Model Applied to Individual Species

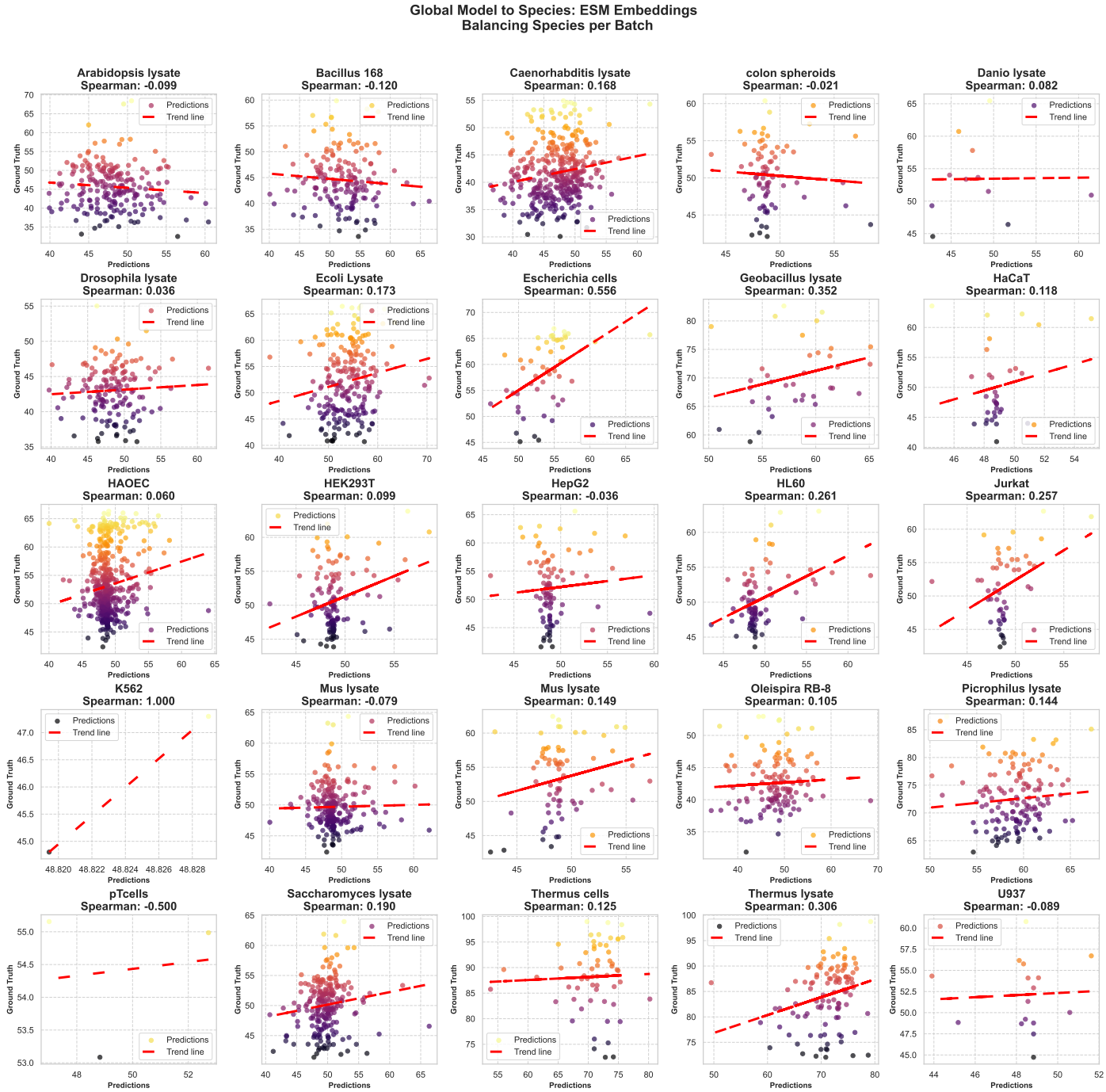

Figure 7: Scatterplot of global model applied to each species using balancing strategy per batch and ESM embeddings

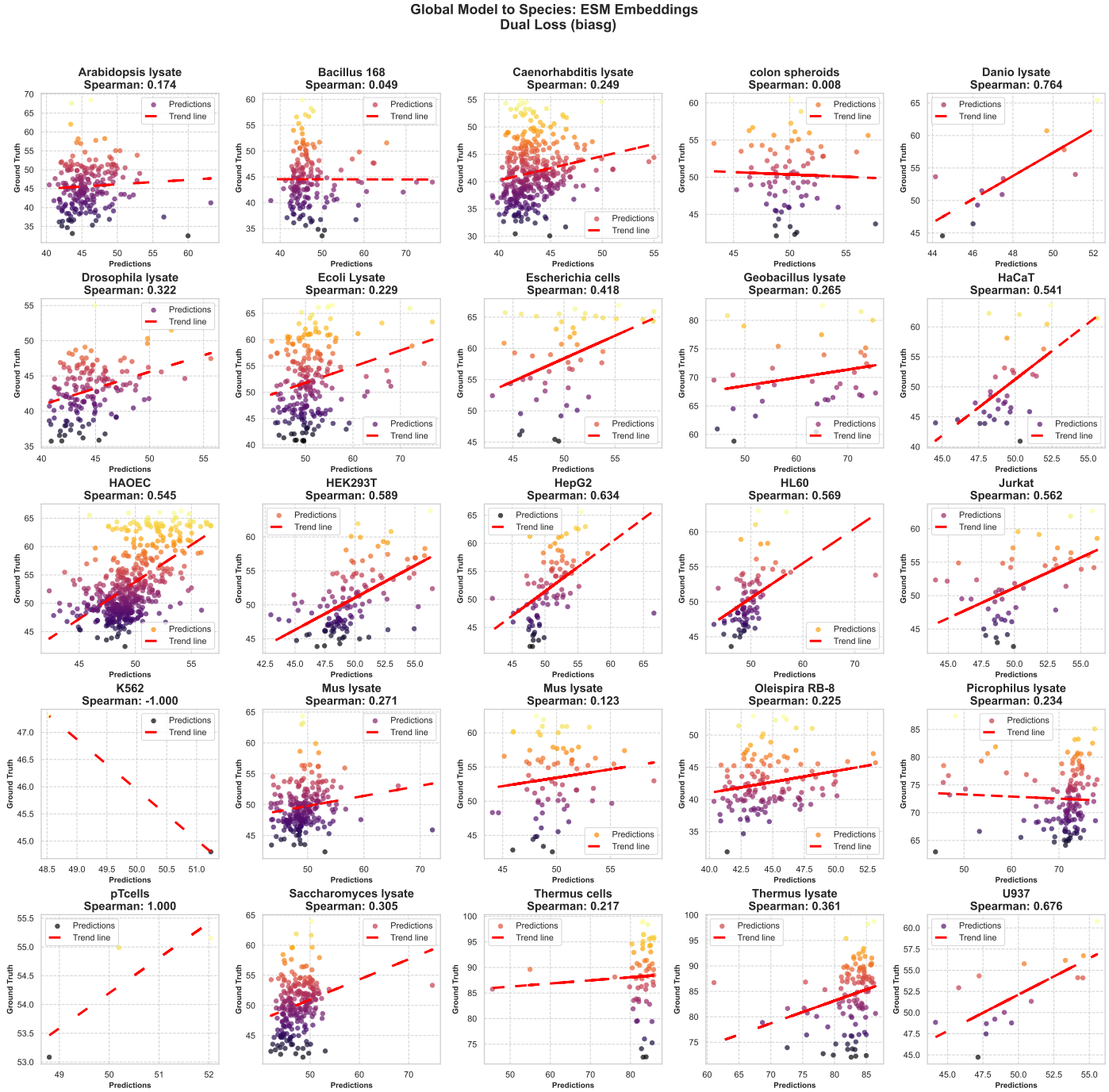

Figure 8: Scatterplot of global model applied to each species using dual loss function and ESM embeddings

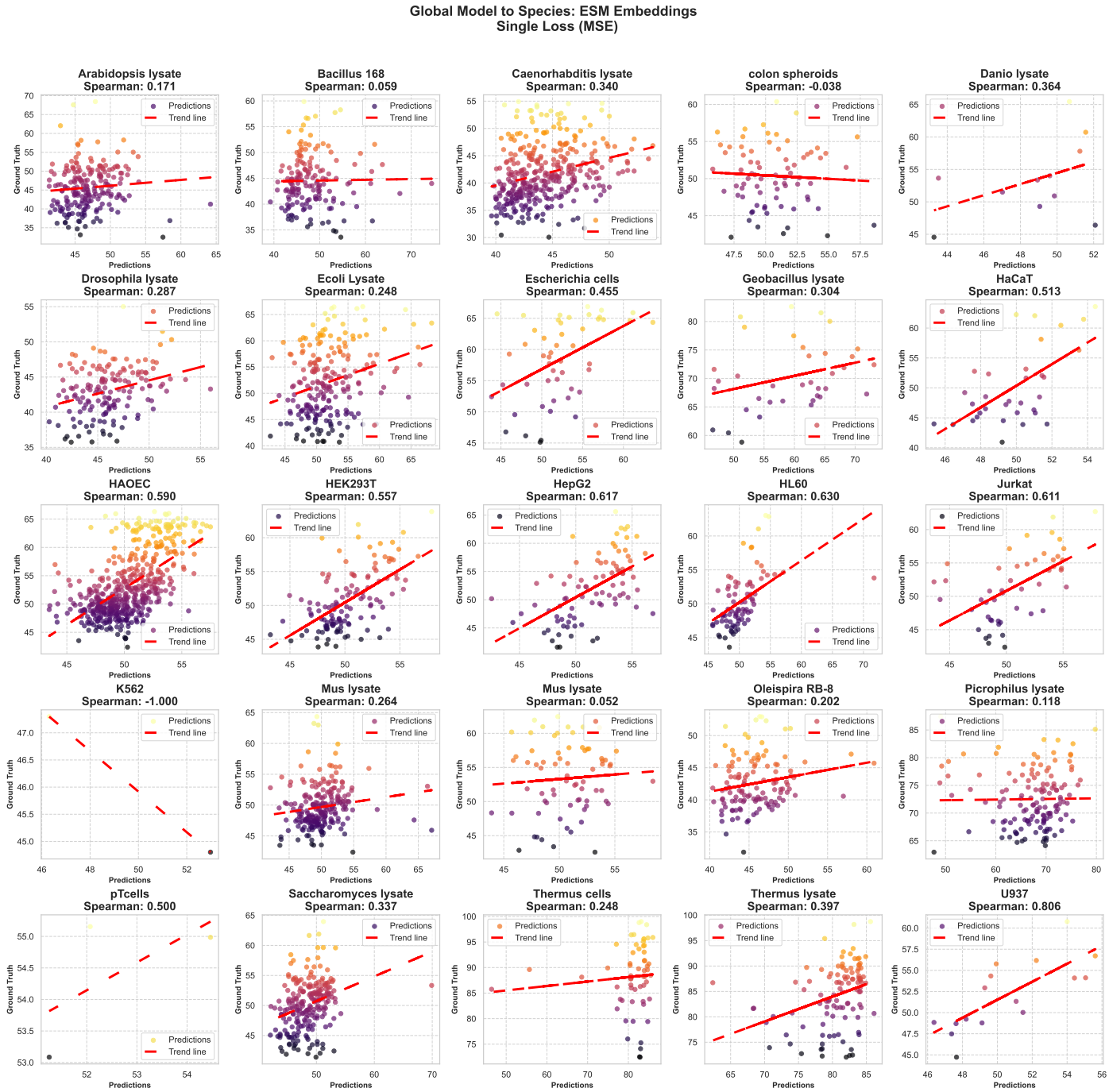

Figure 9: Scatterplot of global model applied to each species using MSE as loss function and ESM embeddings

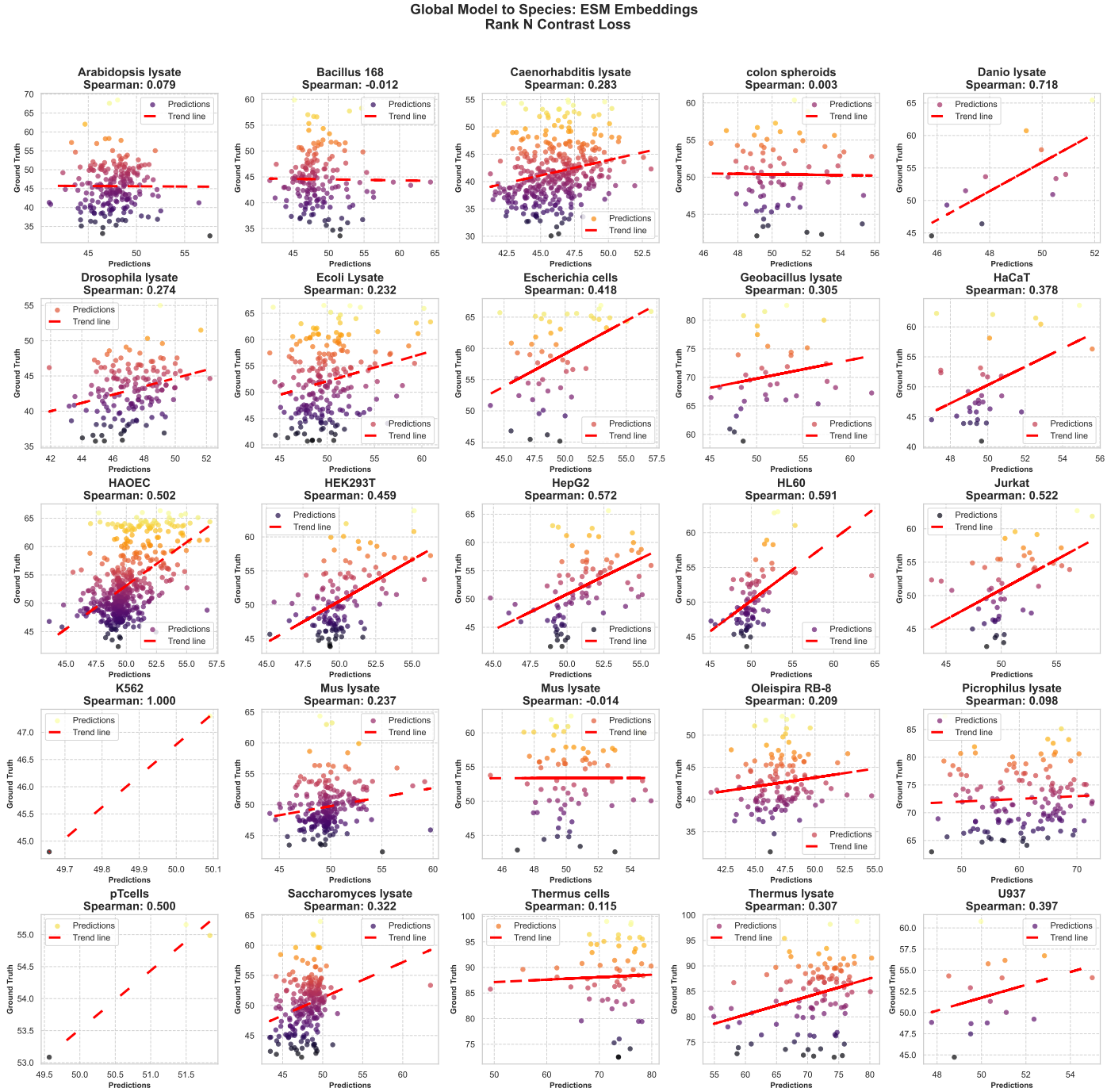

Figure 10: Scatterplot of global model applied to each species using Rank N Contrast loss and ESM embeddings

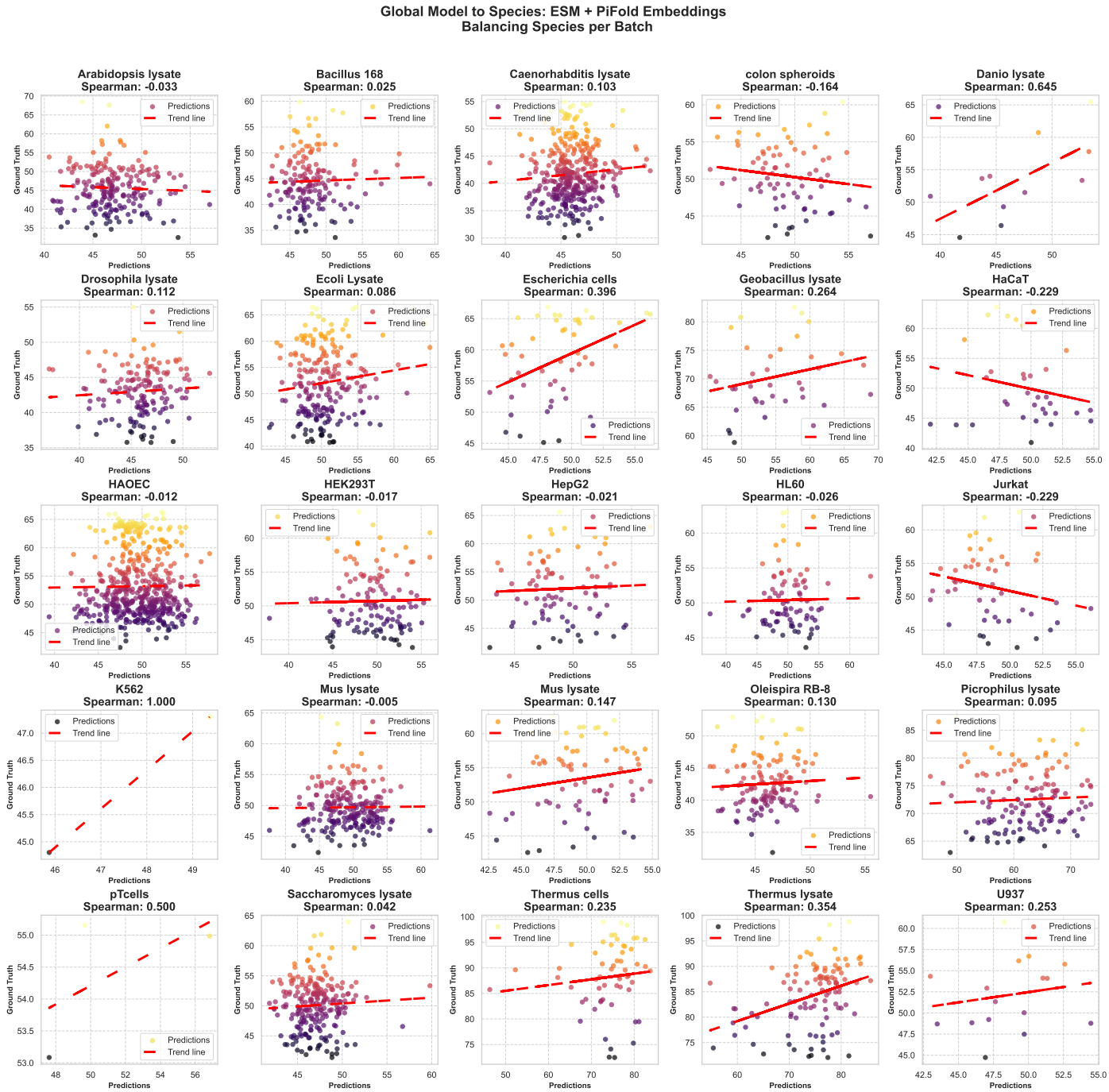

Figure 11: Scatterplot of global model applied to each species using balancing strategy per batch in combination with ESM and PiFold embeddings

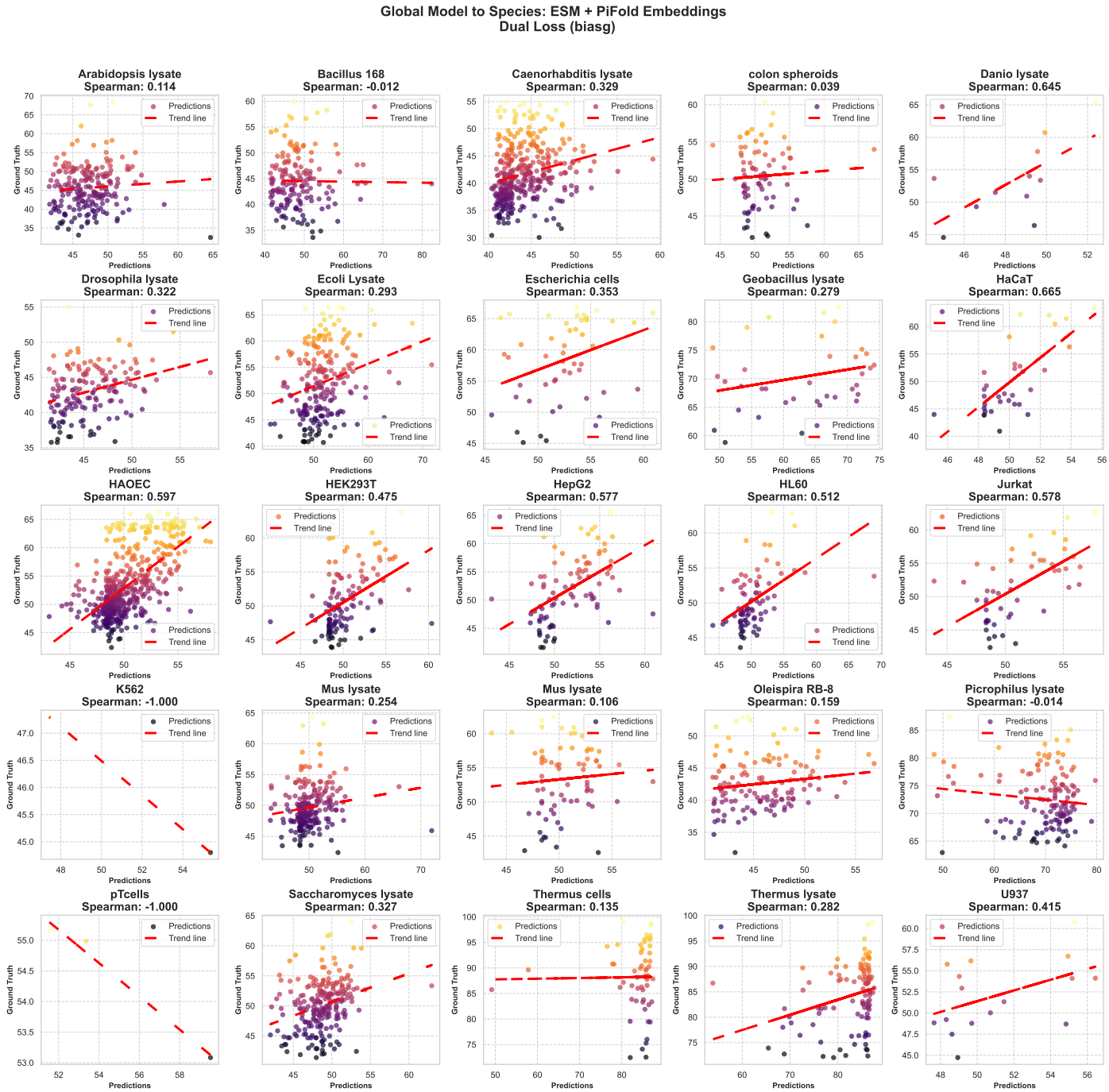

Figure 12: Scatterplot of global model applied to each species using dual loss function in combination with ESM and PiFold embeddings

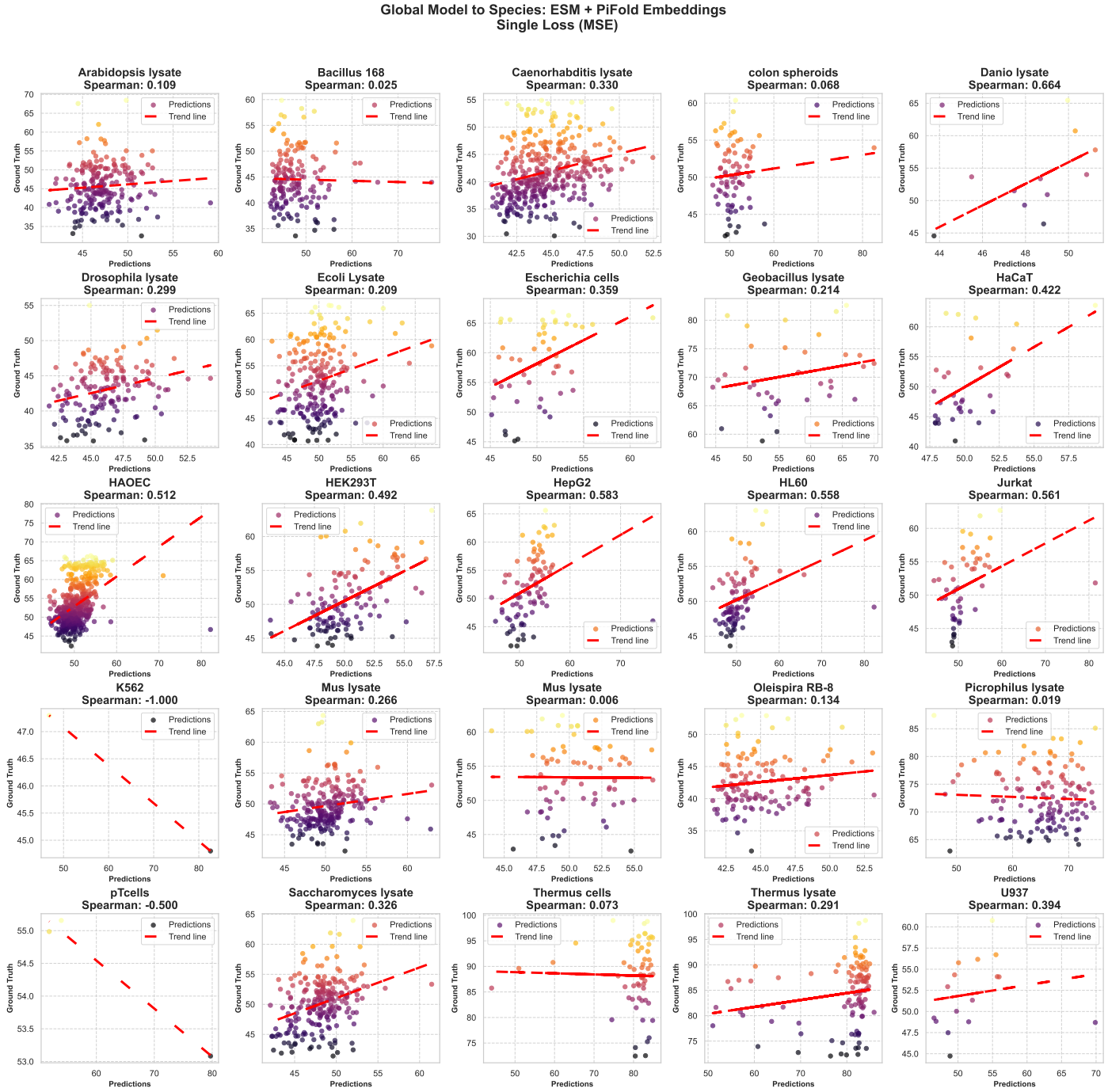

Figure 13: Scatterplot of global model applied to each species using MSE as loss function in combination with ESM and PiFold embeddings

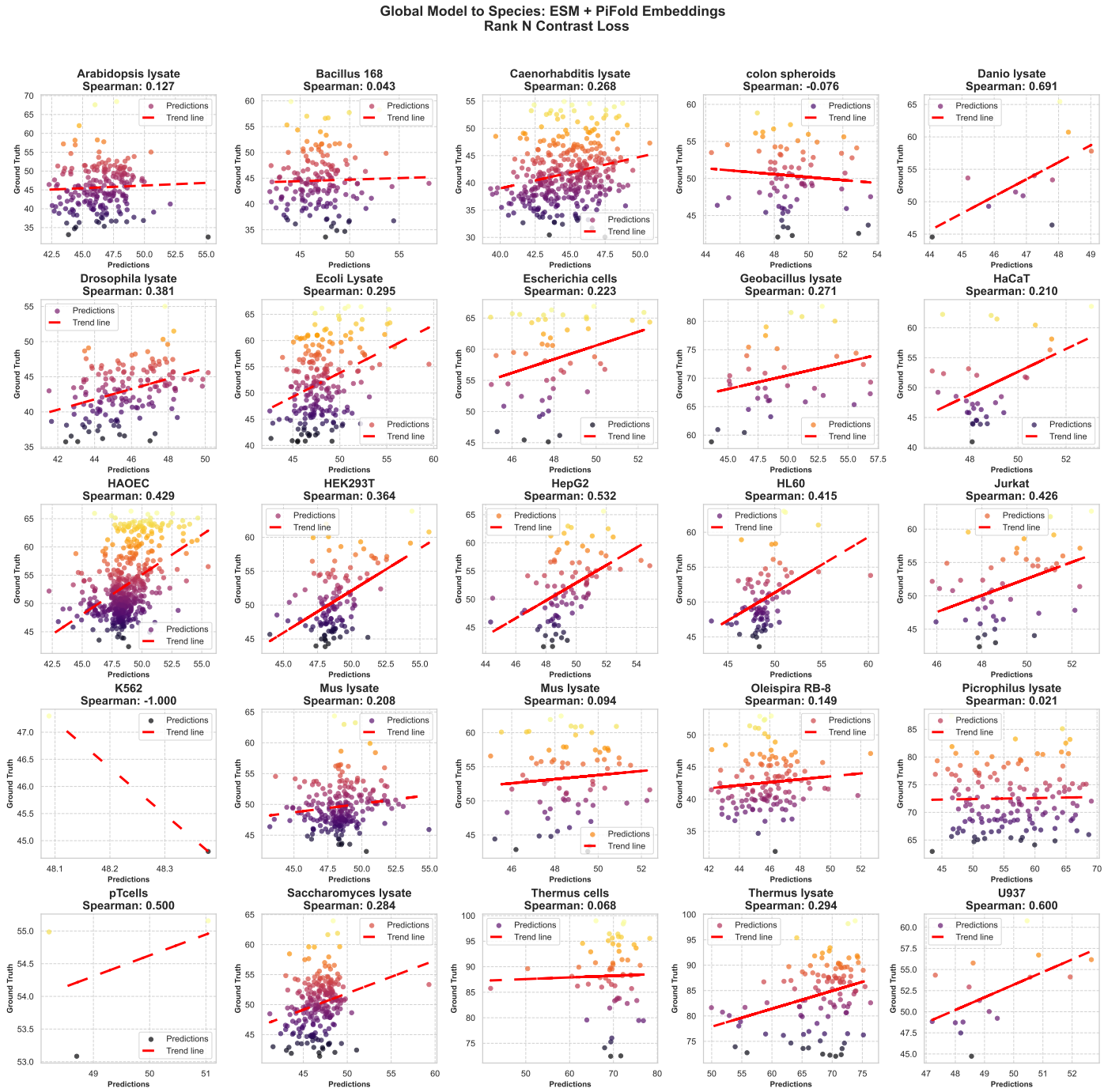

Figure 14: Scatterplot of global model applied to each species using Rank N Contrast loss in combination with ESM and PiFold embeddings

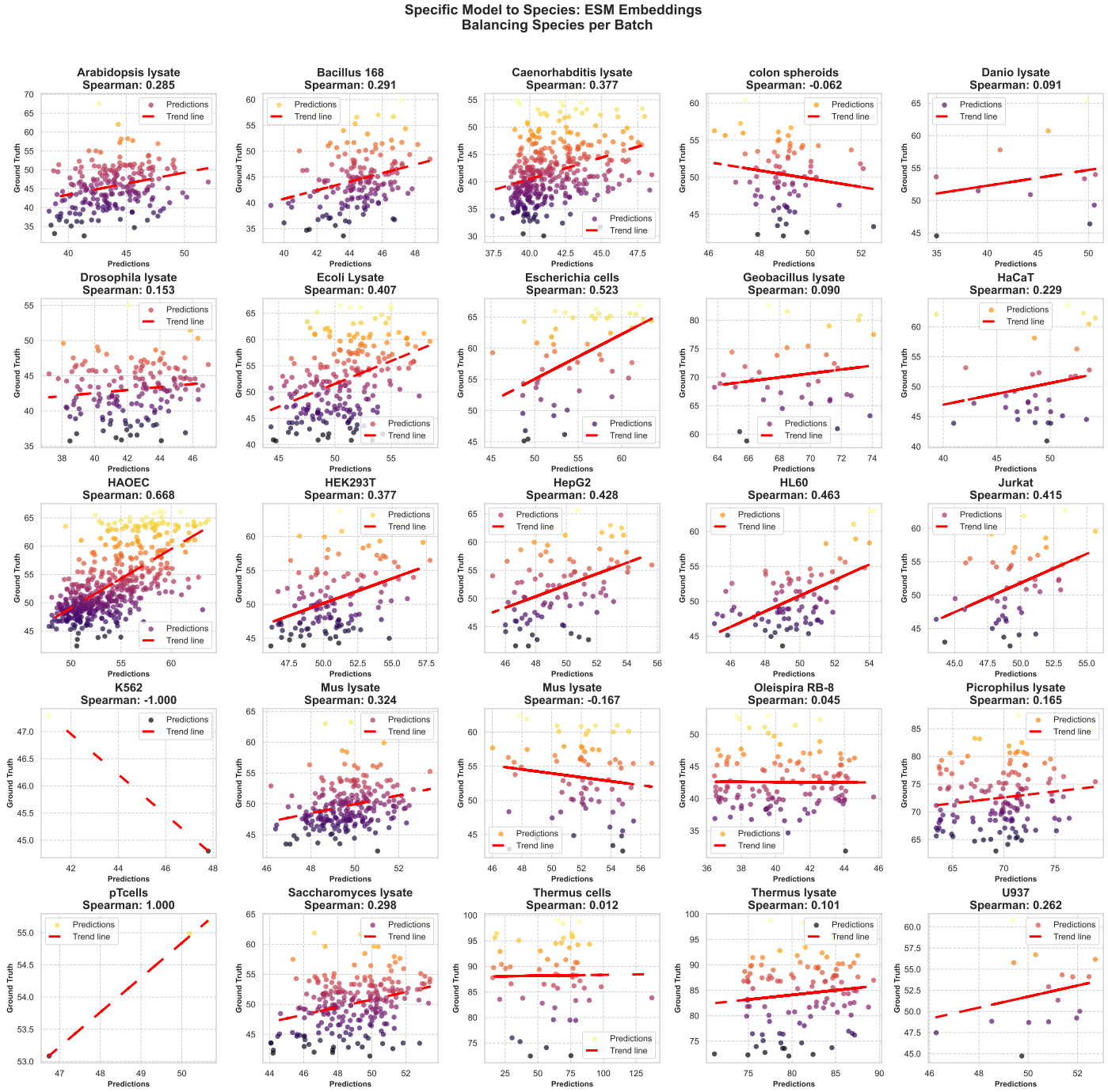

Figure 15: Scatterplot of individual models applied to their target species using balancing strategy per batch with ESM embeddings

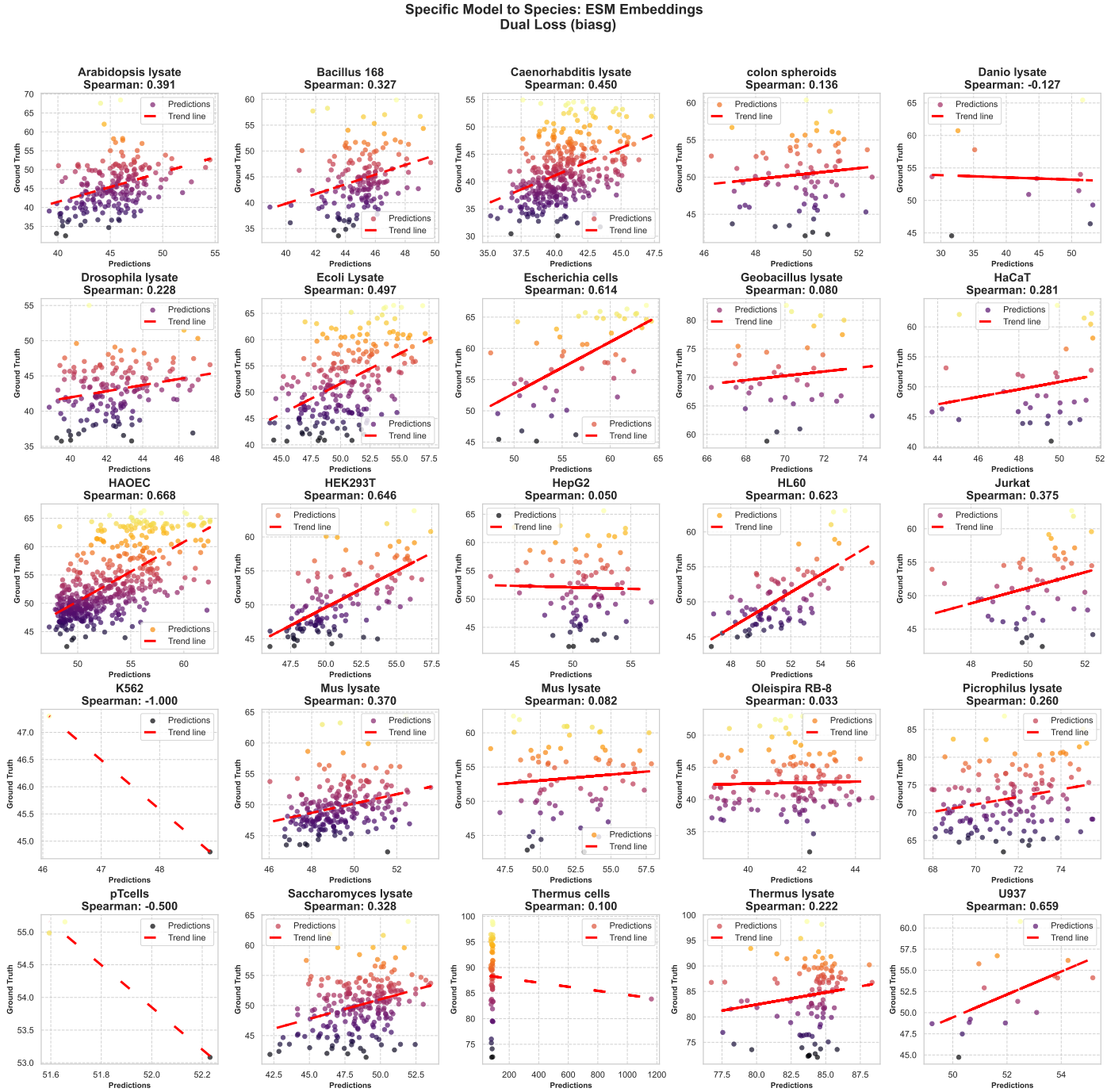

Figure 16: Scatterplot of individual models applied to their target species using dual loss function with ESM embeddings

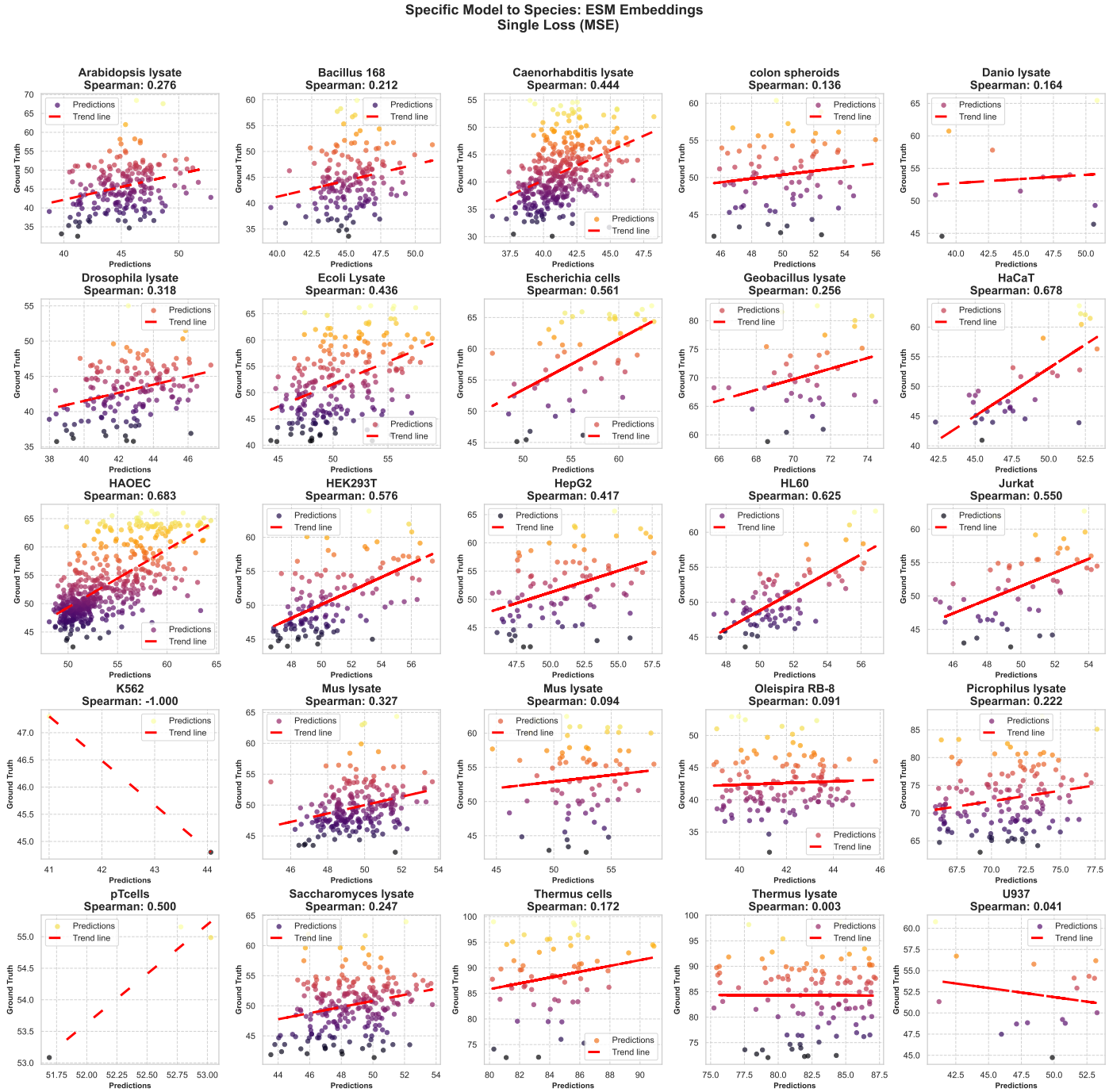

Figure 17: Scatterplot of individual models applied to their target species using MSE as loss function with ESM embeddings

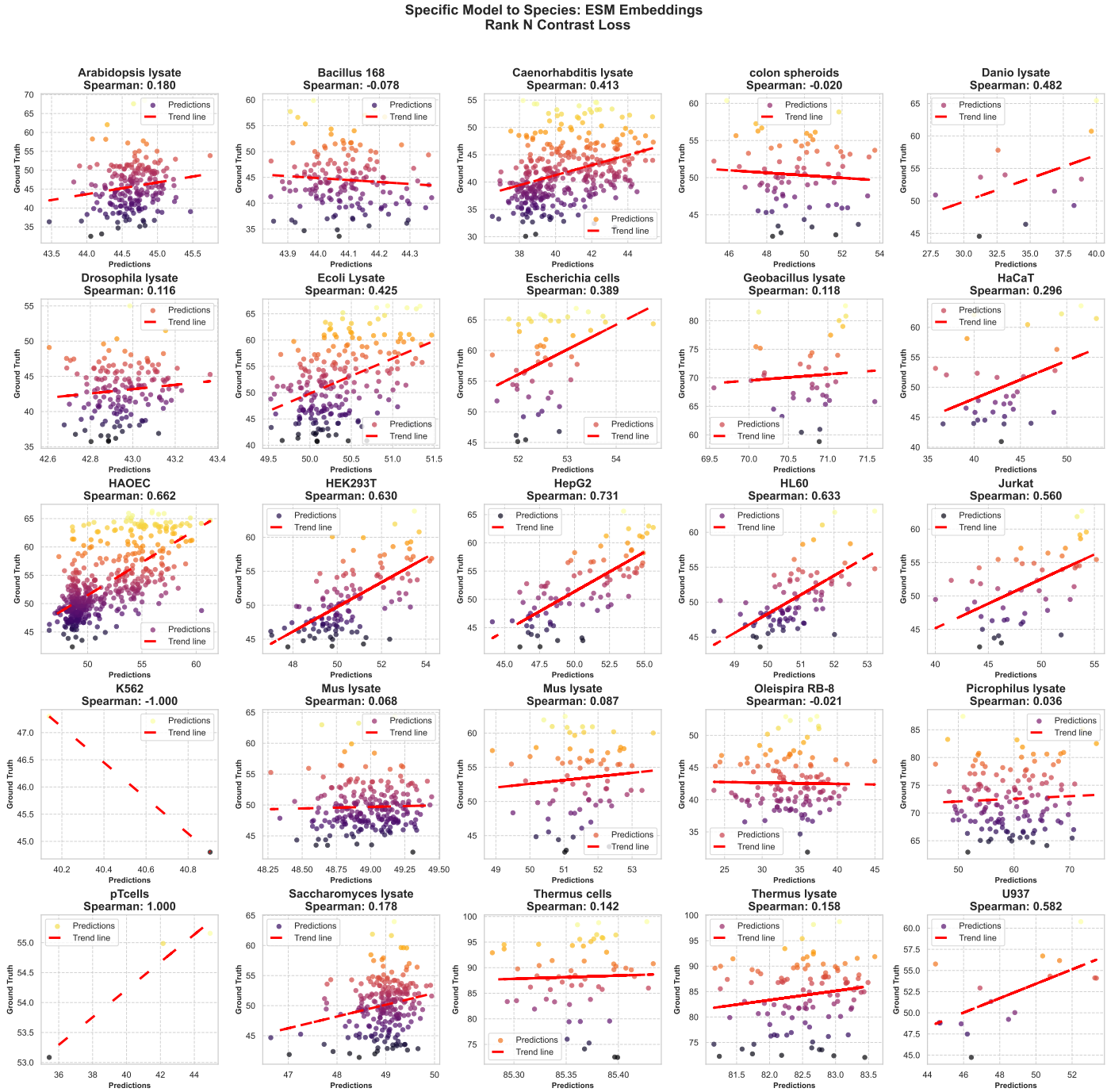

Figure 18: Scatterplot of individual models applied to their target species using Rank N Contrast loss with ESM embeddings

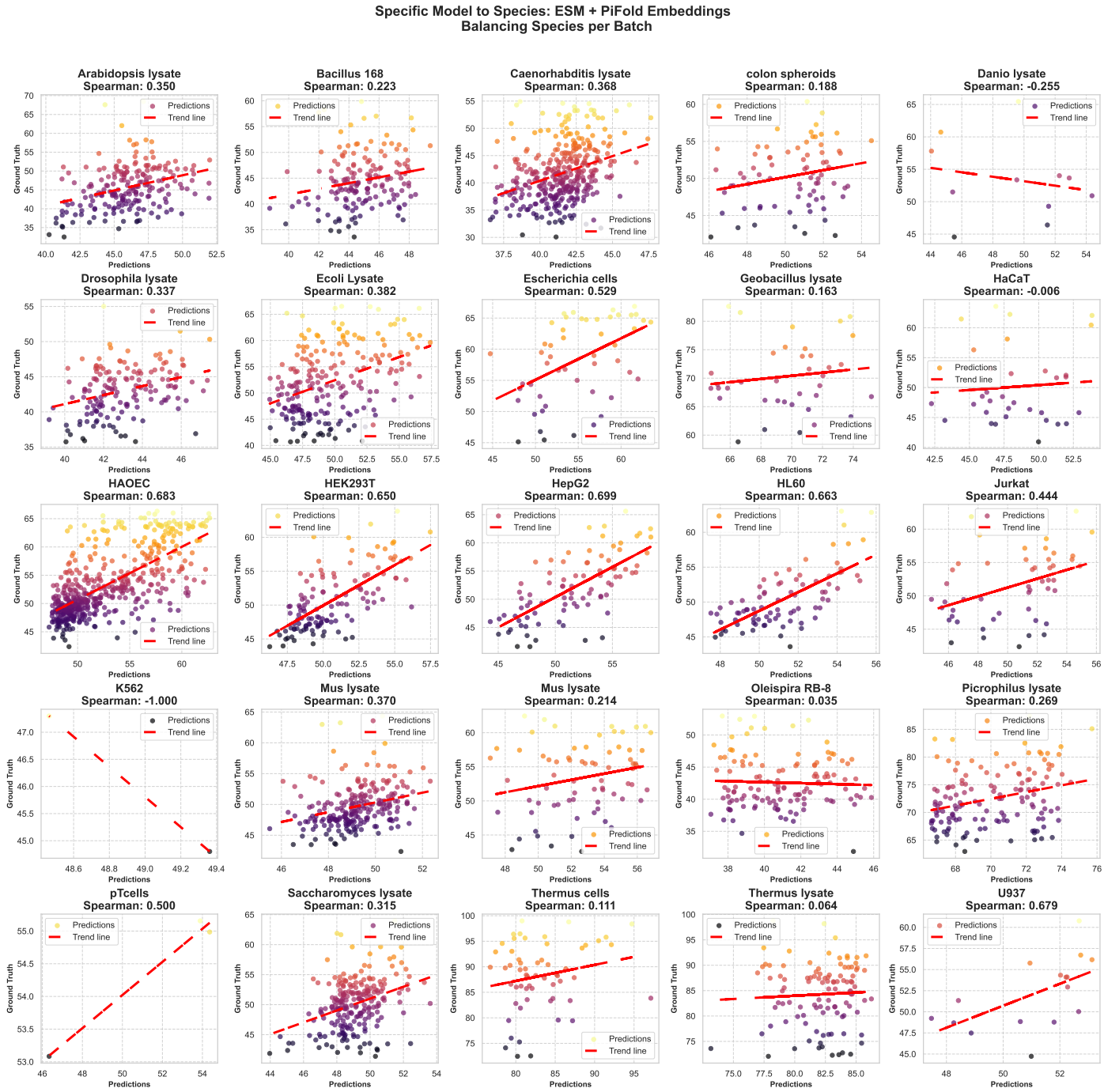

Figure 19: Scatterplot of individual models applied to their target species using balancing strategy per batch in combination with ESM and PiFold embeddings

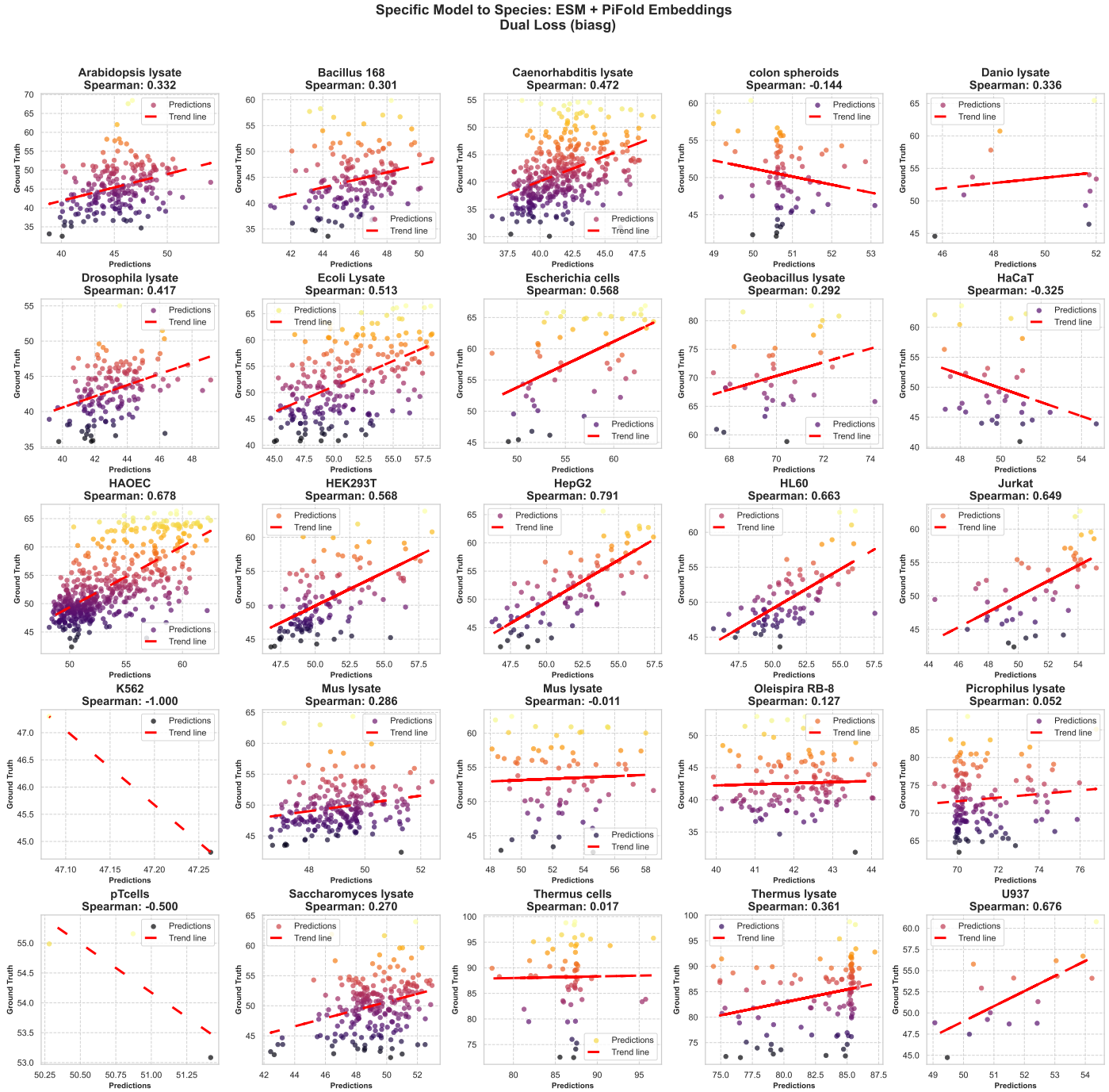

Figure 20: Scatterplot of individual models applied to their target species using dual loss function in combination with ESM and PiFold embeddings

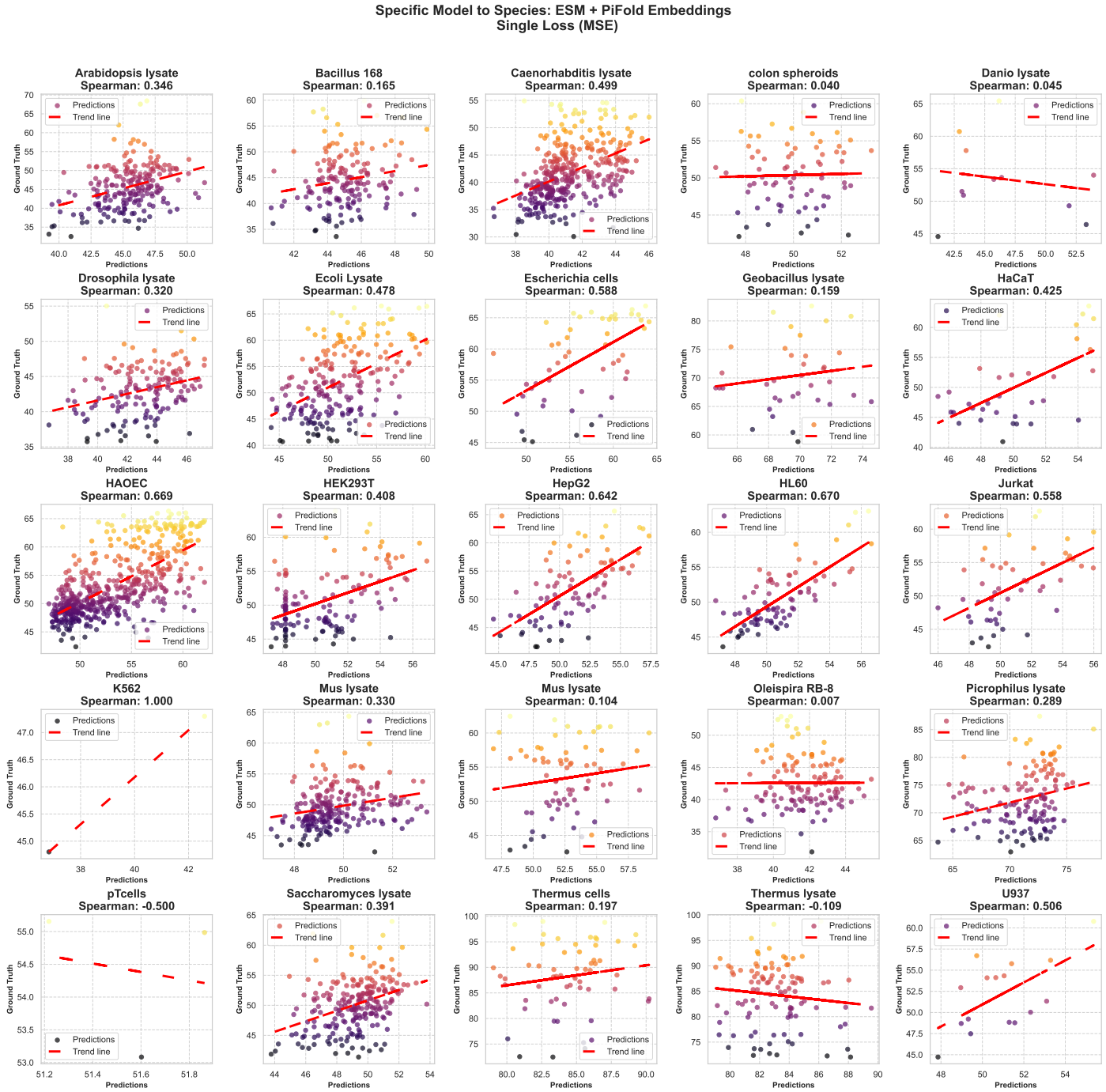

Figure 21: Scatterplot of individual models applied to their target species using MSE as loss function in combination with ESM and PiFold embeddings

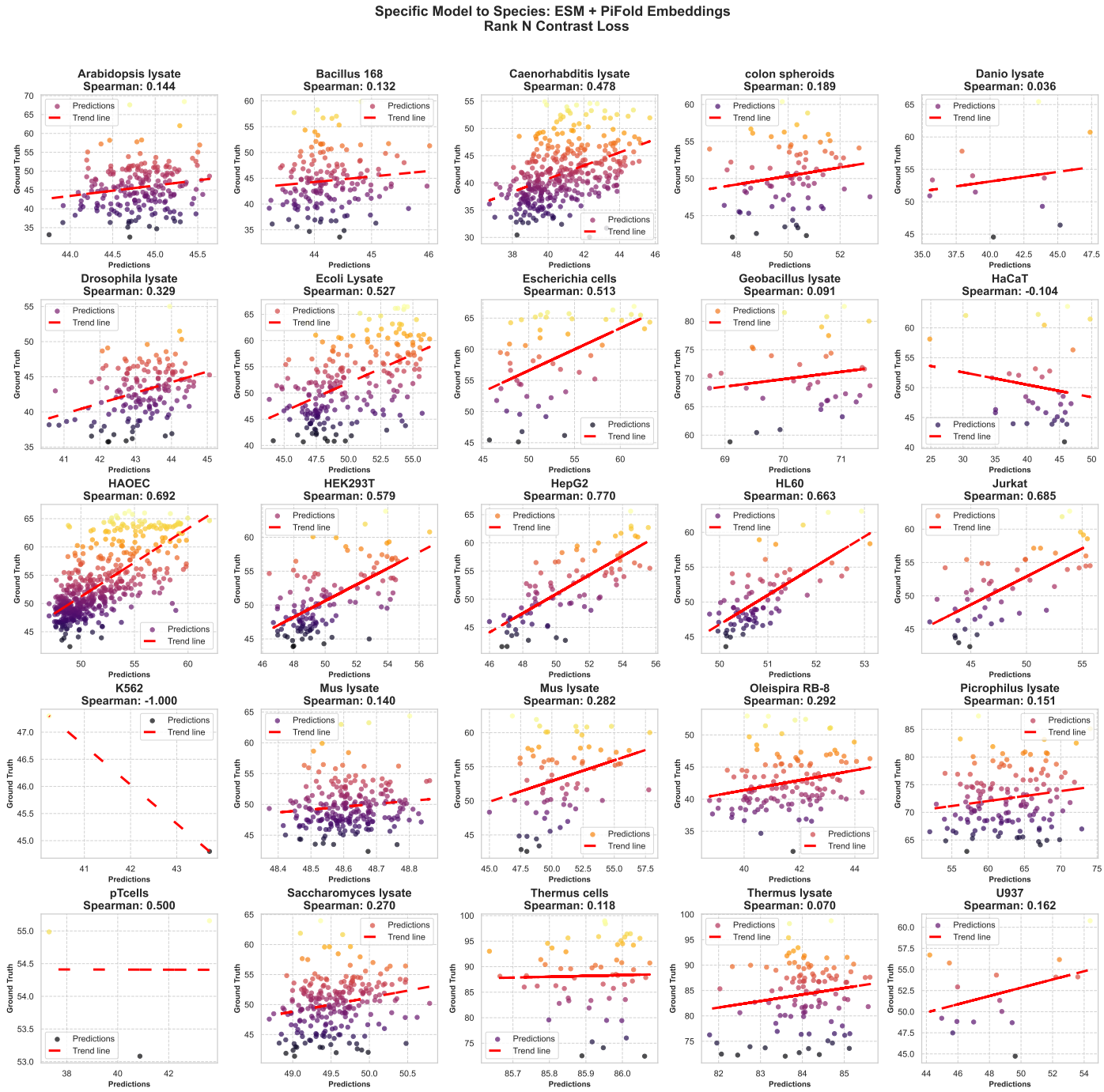

Figure 22: Scatterplot of individual models applied to their target species using Rank N Contrast loss in combination with ESM and PiFold embeddings